ACCEPTED FOR PUBLICATION IN THE ASTROPHYSICAL JOURNAL
Preprint typeset using LaTeX style emulateapj v. 05/12/14

arXiv:1603.07651v1 [astro-ph.SR] 24 Mar 2016

THE *HUBBLE SPACE TELESCOPE* UV LEGACY SURVEY OF GALACTIC GLOBULAR CLUSTERS. VII. IMPLICATIONS FROM THE NEARLY UNIVERSAL NATURE OF HORIZONTAL BRANCH DISCONTINUITIES[1]

T.M. BROWN[2], S. CASSISI[3], F. D'ANTONA[4], M. SALARIS[5], A.P. MILONE[6], E. DALESSANDRO[7], G. PIOTTO[8,9], A. RENZINI[9], A.V. SWEIGART[10], A. BELLINI[2], S. ORTOLANI[8,9], A. SARAJEDINI[11], A. APARICIO[12,13], L.R. BEDIN[9], J. ANDERSON[2], A. PIETRINFERNI[3], AND D. NARDIELLO[8,9]

Accepted for publication in The Astrophysical Journal

ABSTRACT

The UV-initiative *Hubble Space Telescope* Treasury survey of Galactic globular clusters provides a new window into the phenomena that shape the morphological features of the horizontal branch (HB). Using this large and homogeneous catalog of UV and blue photometry, we demonstrate that the HB exhibits discontinuities that are remarkably consistent in color (effective temperature). This consistency is apparent even among some of the most massive clusters hosting multiple distinct sub-populations (such as NGC 2808, ω Cen, and NGC 6715), demonstrating that these phenomena are primarily driven by atmospheric physics that is independent of the underlying population properties. However, inconsistencies arise in the metal-rich clusters NGC 6388 and NGC 6441, where the discontinuity within the blue HB (BHB) distribution shifts $\sim$1,000 K to 2,000 K hotter. We demonstrate that this shift is likely due to a large helium enhancement in the BHB stars of these clusters, which in turn affects the surface convection and evolution of such stars. Our survey also increases the number of Galactic globular clusters known to host blue-hook stars (also known as late hot flashers) from 6 to 23 clusters. These clusters are biased toward the bright end of the globular cluster luminosity function, confirming that blue-hook stars tend to form in the most massive clusters with significant self-enrichment.

Keywords: globular clusters: general – stars: atmospheres – stars: evolution – stars: horizontal branch – ultraviolet: stars

1. INTRODUCTION

Although globular clusters represent the best available laboratories for constraining stellar evolution models, we now know they are not simple stellar populations. Evidence for complex populations are manifested in all phases of stellar evolution. On the main sequence (MS) and red giant branch (RGB), high-precision photometry reveals distinct sequences that are most prominent in massive clusters such as ω Cen (e.g., Anderson 1997; Bedin et al. 2004; Ferraro et al. 2004), NGC 2808 (e.g., D'Antona et al. 2005; Piotto et al 2007; Milone et al. 2015b), M2 (Milone et al. 2015a), and NGC 6715 (e.g., Layden & Sarajedini 2000; Siegel et al. 2007; Piotto et al. 2012), but the phenomenon is apparently universal (Piotto et al. 2012, 2015). The formation mechanisms for these multiple populations remain unclear (see Renzini et al. 2015).

Even before the existence of stellar sub-populations in globular clusters was known, there was considerable evidence for peculiarities in the morphology of the horizontal branch (HB). In particular, there was the well-known "second parameter" problem, first mentioned by Sandage & Wallerstein (1960; see also Sandage & Wildey 1967; van den Bergh 1967); it refers to the observation that parameters other than metallicity (such as age and He abundance) must affect the color distribution of HB stars (see Catelan 2009 for a review). In those clusters where the HB distribution is sufficiently broad in color, a series of discontinuities is also evident, although the appearance of these features varies with the bandpasses employed, manifesting themselves as gaps, jumps, overluminous stars, or subluminous stars. Three prominent examples of such discontinuities are the "Grundahl jump" (G-jump) within the blue HB (BHB) at $\sim$11,500 K (Grundahl et al. 1998, 1999), the "Momany jump" (M-jump) within the extreme HB (EHB) at $\sim$20,000 K (Momany et al. 2002, 2004), and the gap between the EHB and "blue-hook" stars (also known as "late hot flasher" stars; D'Cruz et al. 1996, 2000), spanning $\sim$32,000–36,000 K (Sweigart 1997; Brown et al. 2001). Here we have adopted the usual naming convention for HB stars: EHB stars are those at $T_{\rm eff} \gtrsim$20,000 K, while BHB stars are those hotter

[1] Based on observations made with the NASA/ESA *Hubble Space Telescope*, obtained at the Space Telescope Science Institute, which is operated by the Association of Universities for Research in Astronomy, Inc., under NASA contract NAS 5-26555. These observations are associated with program GO-13297.

[2] Space Telescope Science Institute, 3700 San Martin Drive, Baltimore, MD 21218, USA; tbrown@stsci.edu; jayander@stsci; bellini@stsci.edu

[3] INAF-Osservatorio Astronomico di Teramo, Via Mentore Maggini s.n.c., I-64100 Teramo, Italy; cassisi@oa-teramo.inaf.it; pietrinferni@oa-teramo.inaf.it

[4] INAF-Osservatorio Astronomico di Roma, Via Frascati 33, I-00040 Monteporzio Catone, Roma, Italy; dantona@oa-roma.inaf.it

[5] Astrophysics Research Institute, Liverpool John Moores University, Liverpool Science Park, IC2 Building, 146 Brownlow Hill, Liverpool L3 5RF, UK; M.Salaris@ljmu.ac.uk

[6] Research School of Astronomy and Astrophysics, The Australian National University, Cotter Road, Weston, ACT, 2611, Australia; milone@mso.anu.edu.au

[7] Dipartimento di Fisica e Astronomia, Università degli Studi di Bologna, Viale Berti Pichat 6/2, I-40127 Bologna, Italy; emanuele.dalessandr2@unibo.it

[8] Dipartimento di Fisica e Astronomia "Galileo Galilei", Università di Padova, Vicolo dell'Osservatorio 3, I-35122 Padova, Italy; giampaolo.piotto@unipd.it; sergio.ortolani@unipd.it; domenico.nardiello@unipd.it

[9] INAF-Osservatorio Astronomico di Padova, Vicolo dell'Osservatorio 5, I-35122 Padova, Italy alvio.renzini@oapd.inaf.it; luigi.bedin@oapd.inaf.it

[10] NASA Goddard Space Flight Center, Greenbelt, MD 20771, USA; allen.sweigart@gmail.com

[11] Department of Astronomy, University of Florida, 211 Bryant Space Science Center, Gainesville, FL 32611, USA; ata@astro.ufl.edu

[12] Instituto de Astrofísica de Canarias. Calle Vía Láctea s/n. E38200 - La Laguna, Tenerife, Canary Islands, Spain. aaj@iac.es

[13] University of La Laguna. Avda. Astrofísico Fco. Sánchez, s/n. E38206, La Laguna, Tenerife, Canary Islands, Spain

than the RR Lyrae instability strip (i.e., hotter than ∼8,000 K) but cooler than the EHB. Both Grundahl et al. (1999) and Momany et al. (2004) noted that their respective jumps appear to be ubiquitous features of globular clusters hosting sufficient numbers of BHB and EHB stars, but the surprising consistency of HB gaps in distinct clusters was recognized somewhat earlier (Ferraro et al. 1998). Similarly, the blue-hook phenomenon appears to be common in those clusters hosting an HB population that extends sufficiently far to the blue, but because optical colors become degenerate at the temperatures of EHB stars, UV photometry is needed to confirm their presence (D'Cruz et al. 2000; Brown et al. 2001; Dalessandro et al. 2008; Dieball et al. 2009; Brown et al. 2010).

In a review of hot stars in globular clusters, Moehler (2001) explored various explanations for HB discontinuities, including diverging evolutionary paths, mass loss, distinctions in CNO or rotation rates, dynamical interactions, atmospheric processes, He mixing in red giants, and statistical fluctuations. With time, it has become increasingly clear that atmospheric processes play a dominant role in these HB features. Spectroscopy of stars on either side of the hottest discontinuity demonstrates that, compared to normal EHB stars, blue-hook stars have atmospheres greatly enhanced in He and C (Moehler et al. 2011; Brown et al. 2012), as expected if they formed through a late He core flash that mixed the H-rich envelope with the inner convective regions (a process known as flash mixing; Sweigart 1997; Cassisi et al. 2003). The BHB stars hotter than the G-jump exhibit metal abundances enhanced via radiative levitation, He abundances diminished via gravitational settling (Moehler et al. 1999, 2000; Behr 2003; Pace et al. 2006), and lower surface gravities than expected from canonical BHB models (see Moehler 2001 and references therein). Stellar evolution models that include atomic diffusion have had qualitative success reproducing the observed abundance patterns in BHB stars (Michaud et al. 2007, 2008). Sweigart (2002) first noted that the onset of radiative levitation on the BHB coincided with the disappearance of surface convection. The interplay between atomic diffusion and surface convection was explored more fully by Cassisi & Salaris (2013); they noted that by itself, surface convection should not be enough to suppress radiative levitation in stars cooler than the G-jump, implying that other processes, such as turbulence and rotation, must also play a role.

In addition to abundance differences, there is a clear bimodality in rotation on the BHB (Recio-Blanco et al. 2002, 2004; Behr 2003); stars hotter than the G-jump are generally slow rotators ($v \sin i < 8$ km s^{-1}), while stars cooler than the G-jump are generally fast rotators (with $v \sin i$ as high as 40 km s^{-1}). Although the source of this bimodality remains unclear, Recio-Blanco et al. (2002, 2004) have speculated that the dearth of fast rotators hotter than the G-jump could be due to a loss of angular momentum through stellar winds, driven by the high atmospheric metallicity at such temperatures. Quievy et al. (2009) have argued that meridional circulation in the fast rotators plays a role in the disruption of atomic diffusion in stars cooler than the G-jump.

The consistency of these HB features, and any exceptions to that consistency, are difficult to explore with the heterogeneous observations available in the literature. However, a new catalog of UV and blue photometry, resulting from a *Hubble Space Telescope (HST)* Treasury survey of globular clusters, is well suited to this task (Piotto et al. 2015). In this paper, the seventh in a series associated with the survey, we characterize these HB features in a diverse set of 53 clusters, including clusters with significantly complex populations. We then use these comparisons to explore the implications for the atmospheric phenomena and the evolutionary history of hot stars in globular clusters.

2. DATA

Our analysis employs photometry obtained with the UVIS channel of the Wide Field Camera 3 (WFC3) on board *HST*, largely derived from the UV-initiative Treasury program 13297 (PI: Piotto), but supplemented with data from other Guest Observer programs (e.g., GO-12311, GO-12605; PI Piotto). For ω Cen, we use the photometry of Bellini et al. (2013a, and also in prep.), which draws upon archival WFC3 data, including those from calibration programs. The observations employed the F275W (near-UV), F336W (U), and F438W (B) filters (Figure 1). The Treasury program and data reduction are fully described in Piotto et al. (2015), and the zero-point calibration and differential reddening corrections are detailed in Milone et al. (2015a). Therefore, we will only briefly summarize the observations and data reduction here.

Images from program 13297 were obtained from Aug 2013 to Jun 2015. The data were corrected for charge transfer inefficiency using a pixel-based algorithm developed by Anderson & Bedin (2010) for use with the Advanced Camera for Surveys, but later modified for use with the WFC3. Photometry was performed on each individual exposure using a library of spatially-variable empirical point spread functions, combined into a single measurement for each star, and placed in the VEGAMAG system.

The primary goal of these imaging programs was to study the multiple populations on the MS and RGB. Using observations of NGC 6752, Milone et al. (2013) demonstrated that the multiplicity of globular cluster populations could be distinguished using the color index $C_{\rm F275W,F336W,F438W} = (m_{\rm F275W} - m_{\rm F336W}) - (m_{\rm F336W} - m_{\rm F438W})$; Piotto et al. (2015) subsequently demonstrated the utility of this index in a large set of clusters. For the cool stars on the MS and RGB, the F275W filter includes an OH molecular band, the F336W filter includes an NH molecular band, and the F438W filter includes CN and CH bands (Milone et al. 2012). We will not explore these features here, but they also affect the morphology of the red clump, which falls at similarly cool temperatures.

Although the program was driven by a desire to characterize the MS and RGB, the same UV data provide insight into hot stars in later evolutionary phases. The HB population is well exposed, with photometric errors of ∼0.01 mag and nearly 100% completeness. As on the MS and RGB, the $C_{\rm F275W,F336W,F438W}$ color index is useful for characterizing the HB morphology, but for entirely different reasons (Figure 1). At hotter temperatures, the $(m_{\rm F275W} - m_{\rm F336W})$ color tracks absorption from Fe line blanketing in the near-UV, while the $(m_{\rm F336W} - m_{\rm F438W})$ color spans the Balmer discontinuity, making the $C_{\rm F275W,F336W,F438W}$ index sensitive to atmospheric metallicity and surface gravity in HB stars. Note that these broad-band filters are relatively insensitive to atmospheric He abundance, over the range generally encountered on the HB. Specifically, taking the HB spectra at each of the four temperatures shown in Figure 1, if we decrease the atmospheric Y to 0.01 (simulating the effects of He gravitational settling), or if we increase the atmospheric Y to 0.40 (as associated with a self-enriched sub-population), the variations within each of our bands are $\leq$0.03 mag, and generally ∼0.01 mag (see also Sbordone et al. 2011; Girardi et al. 2007;

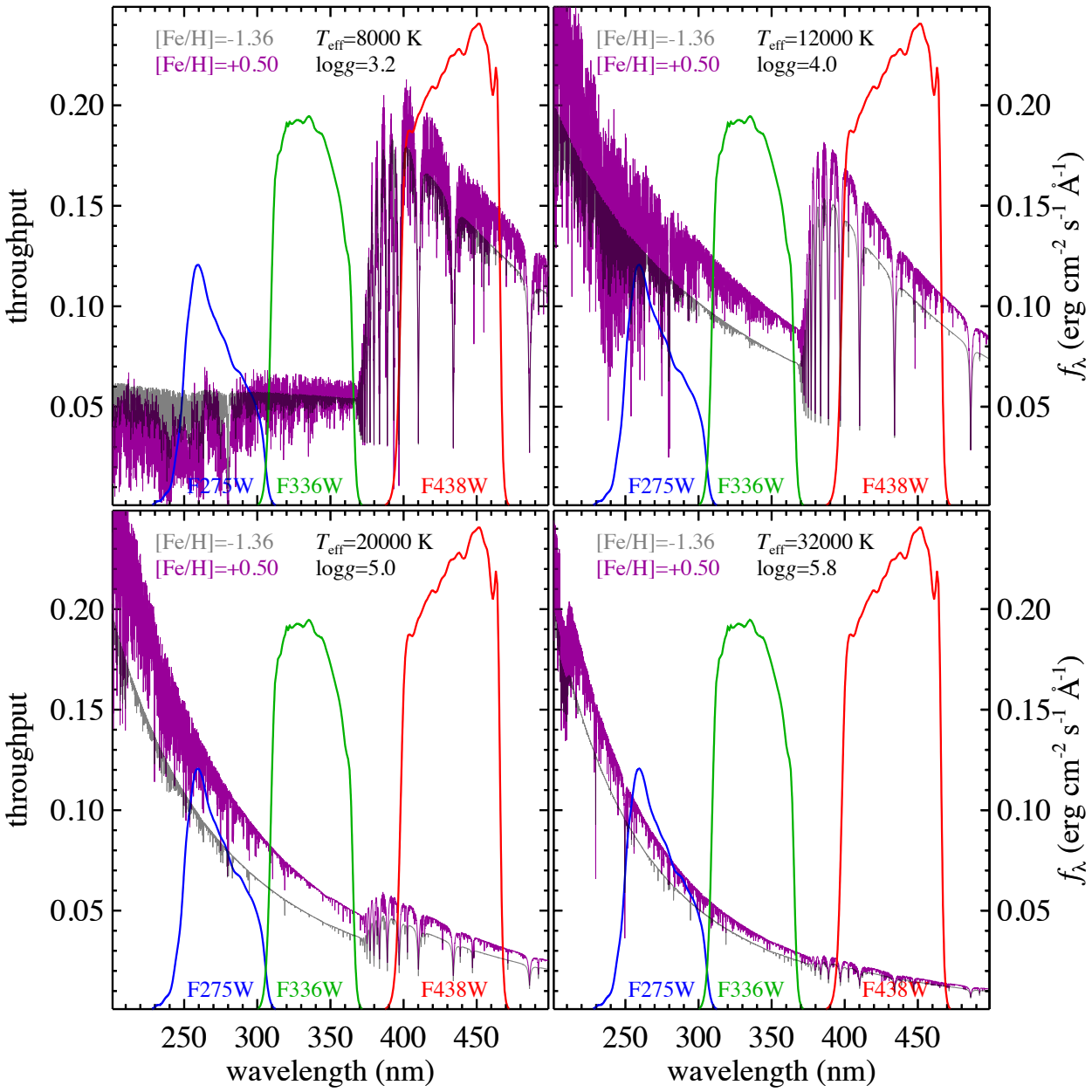

Figure 1. The arbitrarily normalized spectra of four stars along the HB ($T_{\rm eff}$ and surface gravity labeled), at the NGC 2808 metallicity (*grey curve*), compared to the spectra when the metals are enhanced to three times the solar value (*purple curve*). Although we show the effects of metallicity enhancement at each temperature, such enhancements (associated with radiative levitation in the atmosphere) are only observed at temperatures hotter than the G-jump (see text). For comparison, we show the WFC3 bandpasses employed in our analysis: F275W (*blue curve*), F336W (*green curve*), and F438W (*red curve*). The ($m_{\rm F275W} - m_{\rm F336W}$) color tracks absorption from Fe line blanketing in the near-UV, while the ($m_{\rm F336W} - m_{\rm F438W}$) color spans the Balmer discontinuity. The $C_{\rm F275W,F336W,F438W}$ index combines both colors, and is sensitive to both radiative levitation and surface gravity in BHB stars. The high-resolution spectra shown here were calculated using the ATLAS9 and SYNTHE codes (Kurucz 1993; Sbordone et al. 2004), for consistency with the Castelli & Kurucz (2003) spectra used in our analysis.

Dalessandro et al. 2013).

In Figure 2, we show the $C_{\rm F275W,F336W,F438W}$ index alongside the color-magnitude diagram (CMD) of NGC 2808, a massive globular cluster long known to host a peculiar HB morphology (Sosin et al. 1997; Bedin et al. 2000). We highlight three discontinuities in the HB distribution: the G-jump (labeled "G"), the M-jump (labeled "M"), and the gap between the blue-hook stars and the normal EHB (labeled "B"). While these breaks can be discerned in the individual colors comprising the $C_{\rm F275W,F336W,F438W}$ index, they are amplified when the colors are combined in this index. Furthermore, in these crowded fields, the photometric errors are correlated amongst the various bands; in the color-color plane (CCP), these errors are suppressed in both axes, while a CMD will suppress them in only one axis. In addition to these three prominent features, there are small gaps (e.g., at 0.4 mag and 0.8 mag in $m_{\rm F275W} - m_{\rm F438W}$ color), but these do not correspond to features within the HB distributions of the other clusters we will consider here, and could be statistical fluctuations (see, e.g., Catelan et al. 1998). For reference, the peak in the

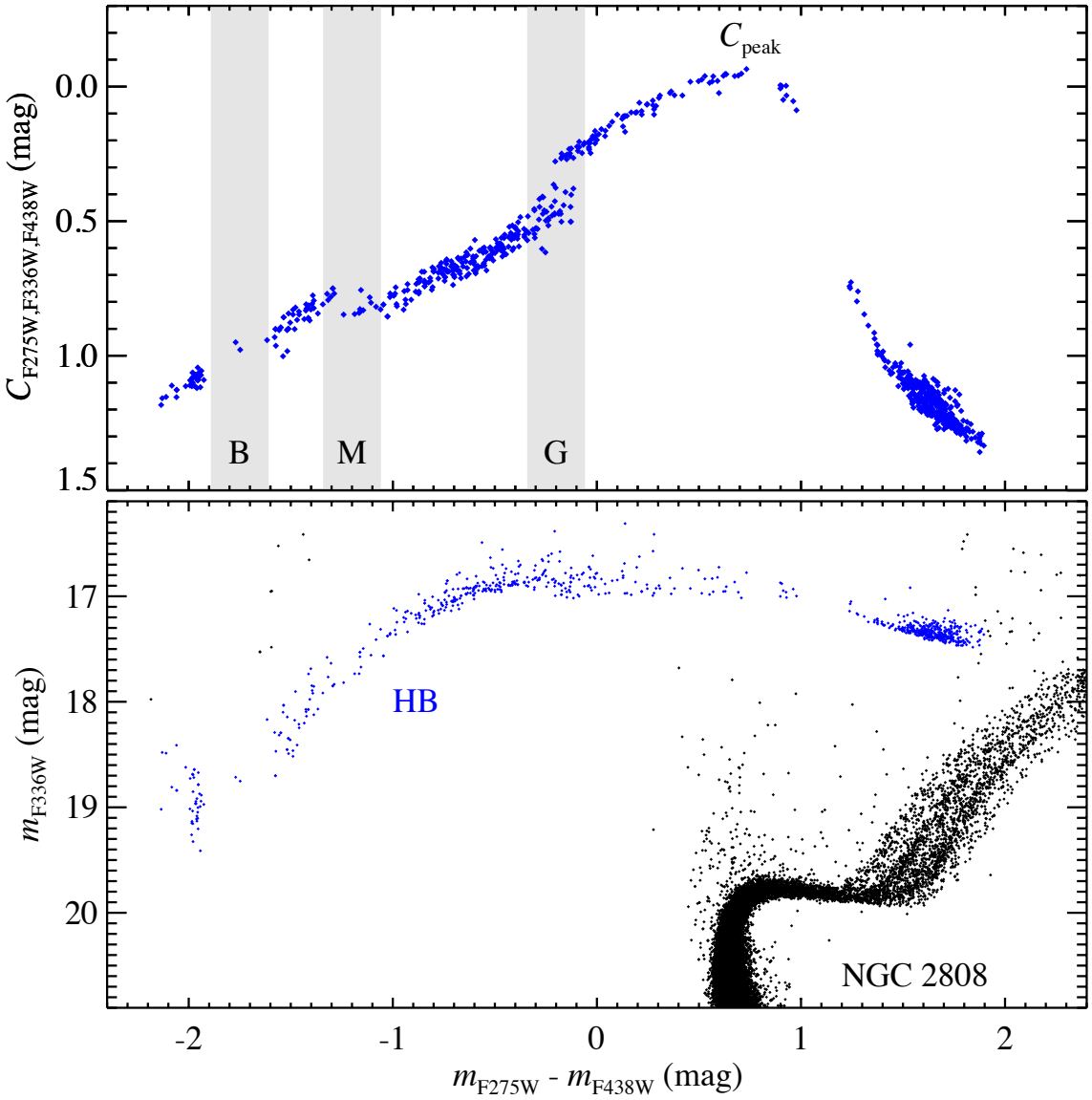

Figure 2. *Bottom panel:* The CMD of NGC 2808 (*points*), highlighting the HB distribution (*blue points, labeled*). *Top panel:* The same HB distribution, but the ordinate has been replaced by the $C_{F275W,F336W,F438W}$ color index. In this CCP, the various HB discontinuities are easily distinguished: the Grundahl jump (G), the Momany jump (M), and the gap between the blue-hook and normal EHB stars (B). The large gap to the red of the Grundahl jump is the RR Lyrae instability strip. We use the peak in the $C_{\rm F275W,F336W,F438W}$ index (*labeled*) to align HB distributions to each other and to models.

$C_{\rm F275W,F336W,F438W}$ index corresponds to an effective temperature of ∼8,600 K, driven primarily by the sensitivity to the Balmer discontinuity in the $(m_{\rm F336W} - m_{\rm F438W})$ component of the index. This peak is well-defined in the CCP, falls in the middle of the HB color range, and is populated in nearly all of the clusters in our sample, so we shall use it as a reference point, hereafter called $C_{\rm peak}$.

3. ZERO-AGE HORIZONTAL BRANCH MODELS

The ZAHB models of Brown et al. (2010) that are used in the present paper were computed with a highly-modified version of the original Princeton stellar evolution code (Schwarzschild & Härm 1965). This code has been extensively updated over the years (Sweigart & Demarque 1972; Sweigart & Gross 1974, 1978; Sweigart 1987, 1997). The equation of state (EOS) is based on a tabulation of the Fermi-Dirac integrals and the various thermodynamic functions for both the non-relativistic and relativistic regimes. At low temperatures, the EOS solves the Saha equation for the ionization of H and He, as well as the first ionization of 10 heavy elements, plus the formation of H_2. The code also incorporates the OPAL radiative opacities of Rogers & Iglesias (1992), while at low temperatures, the molecular opacities of Bell (1995, private communication) are used. The nuclear reaction rates are taken from Caughlan & Fowler (1988), except for the $^{12}C(\alpha, \gamma)^{16}O$ reaction, where the higher rate suggested by Weaver & Woosley (1993) has been adopted. A further discussion of the input physics in our evolution code can be found in the description of the related PGPUC code of Valcarce et al. (2012).

This code has also been highly automated and, as a result, can follow the evolution of a globular-cluster star continuously from the MS up the RGB and then through the He-core flash, HB, and asymptotic-giant branch phases in a single

computer run. For example, all of the HB sequences in Brown et al. (2010) were evolved continuously through the He flash, thereby avoiding the need to construct separate ZAHB models. Convective overshooting and semi-convection in our HB models have been treated according to the method of Robertson & Faulkner (1972). This method is applied between iterations of the Henyey method and ensures that the radiative and adiabatic gradients agree to better than 10^{-4} at the convective-core edge and within the semi-convective zone in the final converged models. In addition, the mixing length in our evolution code was calibrated by requiring that a solar model reproduce the solar luminosity and radius as well as the solar Z/X ratio at an age of 4.6 Gyr.

4. ANALYSIS

4.1. *Empirical Comparisons*

For our analysis, we will use the HB distribution of NGC 2808 as an empirical template for inspecting the HB distributions of the other clusters in the survey. This might seem like an unusual choice, because NGC 2808 is not at all representative of the Milky Way globular cluster system, being one of the most massive (M_V = –9.4 mag; Harris 1996), with distinct MS and RGB sequences (D'Antona et al. 2005; Piotto et al. 2007; Milone et al. 2015b) and prominent HB gaps (Bedin et al. 2000). However, the HB of NGC 2808 is well-populated across the full range of temperature, with stars in the red clump, BHB, EHB, and blue hook (Figure 2). If any of its HB features are the result of universal atmospheric phenomena, as opposed to a product of the multiple populations driving the MS and RGB splitting, then these features should align with those present in the HB distributions of other clusters, as long as the corresponding HB locations are populated.

Given the prominence of the discontinuities in the CCP of Figure 2, it is useful to compare the HB distribution of each cluster to that of NGC 2808 in this plane. Distance is not a factor in a CCP, but extinction is; we need to align the HB distributions with a fiducial that is independent of the HB discontinuities we are investigating. We use the $C_{\rm peak}$ for this purpose, which is well-populated in nearly all of our clusters. The only exceptions are 9 clusters with HB stars lying entirely in the red clump; for completeness, we will include them here, and align them to NGC 2808 at the red clump, but their lack of stars hotter than the RR Lyrae instability strip makes them irrelevant to the investigation of HB discontinuities.

A possible concern when making these empirical comparisons to NGC 2808 is that simple shifts within the CCP are implicitly making the assumption that the extinction vector is independent of spectral energy distribution (SED). Because the photometry here covers a broad wavelength range from the near-UV to the B band, and because the HB stars in question span a broad temperature range of ∼5,000–40,000 K, this assumption is not entirely correct, but in fact the approximation is sufficient for the purpose of making empirical comparisons between the clusters. This is true even though our survey includes halo clusters with almost no foreground reddening and bulge clusters with significant reddening. The difference in foreground reddening for any cluster of our survey, when compared to that of NGC 2808, can be as large as 0.5 mag in $E(B-V)$. To demonstrate the validity of this approximation, we show in Figure 3 stellar structure models for the zero-age HB (ZAHB) in NGC 2808 (Brown et al. 2010), which assumed [Fe/H]=–1.36 (Walker 1999) and no He enhancement[14] (i.e., $\Delta Y = 0$), transferred to the CCP using the LTE synthetic spectra of Castelli & Kurucz (2003) and the WFC3 bandpass throughputs. In one case (*solid blue curve*), unreddened synthetic spectra were used to transfer the structure models to the observable plane, and then shifted to align at the $C_{\rm peak}$. In the other case (*dashed red curve*), the structure models were transferred to the observable plane using spectra that were reddened with the Fitzpatrick (1999) extinction curve, assuming $E(B-V) = 0.5$ mag, and then shifted to align at the $C_{\rm peak}$. The deviation of the observations below the theoretical ZAHB curves between the G-jump and M-jump, due to radiative levitation, will be explored extensively below. The two curves agree with each other perfectly in the middle of the HB range (by definition), but separate as one looks to the red and blue extremes of the HB. However, the distinctions between the models are small: at the location of the G-jump, using either the red curve or the blue curve to estimate the effective temperature of the G-jump would only change the estimate by 100 K (0.02 mag change in $m_{\rm F275W}-m_{\rm F438W}$), while at the location of the M-jump, the temperature estimates would only differ by 500 K (0.04 mag change in $m_{\rm F275W}-m_{\rm F438W}$). Thus, even when comparing HB distributions of clusters with significantly distinct foreground reddening, the agreement in the colors of these features implies agreement in their temperatures at the level of ∼500 K or less. In cases where the colors of these discontinuities do not agree between clusters, their temperatures can be quantified with a theoretical ZAHB distribution tailored to match the cluster in question, including an SED-dependent foreground extinction.

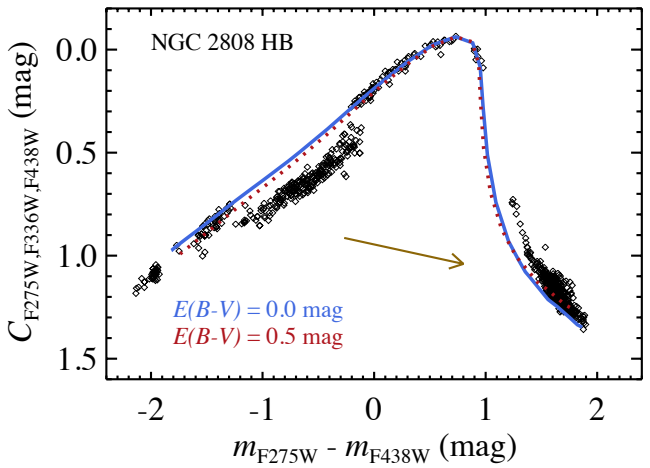

Figure 3. The observed HB distribution of NGC 2808 (*black points*) in the CCP that highlights its HB discontinuities. The extinction vector for a 12,000 K BHB star is shown (*brown arrow*). Strictly speaking, the extinction vector in this plane is SED dependent. However, for the purposes of empirical comparisons to the other clusters in our sample, one can assume an SED-independent extinction vector and simply shift the HB distribution of any cluster to align with that of NGC 2808, using the $C_{\rm peak}$ as a fiducial. We demonstrate the accuracy of this approach by shifting a theoretical ZAHB distribution to align with the observations at the $C_{\rm peak}$, using two different extinction assumptions. In one case, no foreground reddening was applied before the alignment (*solid blue curve*), and in the other, significant SED-dependent reddening was applied before the alignment (*dotted red curve*), but the distinction between the two curves is small. The deviation of the observed BHB below the ZAHB curves at $-1.2 < (m_{\rm F275W}-m_{\rm F438W}) < -0.2$ mag is due to radiative levitation blueward of the G-jump. The stars falling to the blue of the ZAHB curves, at $(m_{\rm F275W}-m_{\rm F438W}) < -1.8$ mag, are blue-hook stars, with effective temperatures hotter than the canonical end of the EHB.

[14] Enhancement is relative to stars born on the MS with a primordial He abundance of $Y = 0.23$.

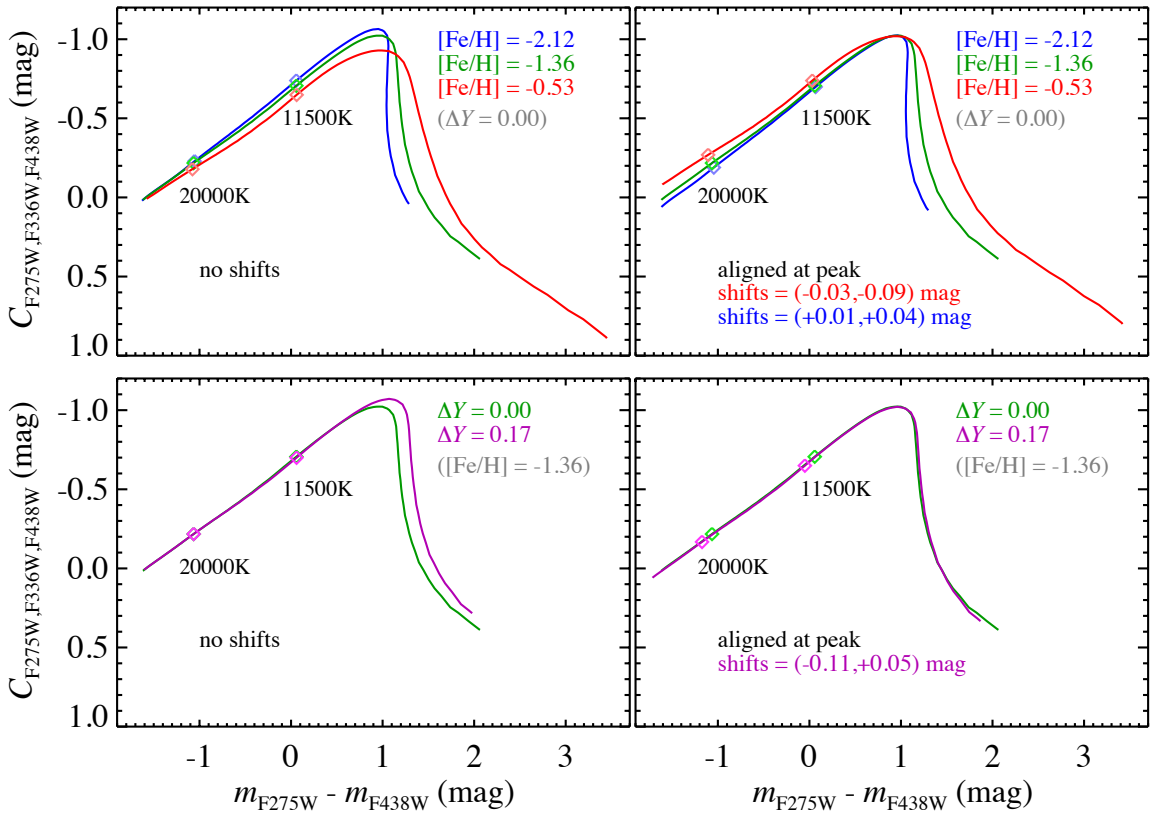

Figure 4. Theoretical ZAHB models (*curves*) before (*left panels*) and after (*right panels*) they are aligned at the $C_{\rm peak}$, for variations in metallicity (*top panels*) and He abundance (*bottom panels*). The $C_{\rm peak}$ reference point on the BHB falls at 8,600±100 K, and this holds true over the range of $-0.53 \leq$ [Fe/H] -2.12 and over the range of $0 \leq \Delta Y \leq 0.17$. Although NGC 2808 is an unusually massive cluster, its abundance profile and well-populated HB make it a useful template population; the BHB stars of NGC 2808 fall in the middle of these abundance ranges, with intermediate metallicity ([Fe/H] = −1.36; Walker 1999), and moderate He enhancement ($\Delta Y \sim 0.09$; Marino et al. 2014). Using $C_{\rm peak}$ to align the HB distribution of any cluster in our sample to that of NGC 2808 should give agreement at the G-jump and M-jump, at the level of 0.06 mag (or better) in $m_{\rm F275W} - m_{F438W}$ color, unless the temperatures of these features are not universal.

Another possible concern when comparing observed HB distributions to that of NGC 2808 is the effect of abundance distinctions between clusters. Fortunately, ZAHB models demonstrate that the intrinsic $m_{\rm F275W} - m_{\rm F438W}$ color is not very sensitive to Y or [Fe/H] at the effective temperatures of the $C_{\rm peak}$ (∼8,600 K), the G-jump (∼11,500 K), or the M-jump (∼20,000 K), as demonstrated in Figure 4. In the top panels, we show the effects of [Fe/H]; in the bottom panels, we show the effects of Y. In the left panels, we show the ZAHB distributions at their relative positions in the CCP, before any alignments are made; in the right panels, we show the ZAHB distributions after they have been aligned at the $C_{\rm peak}$ reference point. Because NGC 2808 is of intermediate metallicity ([Fe/H] = −1.36; Walker 1999), using the $C_{\rm peak}$ to align clusters of either high or low metallicity incurs misalignments in $m_{\rm F275W} - m_{\rm F438W}$ color of less than 0.05 mag at the G-jump and M-jump. Because the BHB stars near the $C_{\rm peak}$ in NGC 2808 are only moderately enhanced in He ($\Delta Y \sim 0.09$; Marino et al. 2014), using the $C_{\rm peak}$ to align clusters with little He enhancement or strong He enhancement incurs misalignments in $m_{\rm F275W} - m_{\rm F438W}$ color of less than 0.06 mag at the G-jump and M-jump, which corresponds to a $T_{\rm eff}$ difference of 240 K at the G-jump and 740 K at the M jump. If the systematic errors from [Fe/H] and Y went in the same direction, the misalignment could be as large as 0.1 mag.

In Figure 5, we compare the HB distribution of NGC 2808 (*grey points*) to that of each of the other 52 clusters in our sample (*blue points*). Each of the HB distributions has been aligned to that of NGC 2808 at the $C_{\rm peak}$, accounting for distinctions in composition and extinction. To aid these comparisons, the 52 clusters have been sorted into five arbitrary categories (explained below) with increasingly blue HB morphology. Within each category, we also sort the clusters by the mean $(m_{\rm F275W} - m_{\rm F438W})$ color of the 10 bluest HB stars in each cluster, after the cluster HB has been aligned to that of NGC 2808 (otherwise it would depend upon both HB morphology and extinction). The choice of sorting metric is arbitrary, but our chosen metric is more useful than other obvious choices, such as the color of the single bluest star (which is hampered by outliers) or the mean color of the entire HB (which is affected by strongly bimodal HB distributions). Of the 52 clusters compared to NGC 2808, 17 do not host sufficiently blue HB stars to characterize the three HB discontinuities blueward of the RR Lyrae instability strip. Of the remaining 36 clusters, all but two (NGC 6388 and NGC 6441) exhibit excellent agreement with the discontinuities observed in NGC 2808, although the varying HB morphologies of these clusters do not always lend themselves to exploring each feature in detail. Furthermore, the red clump in these clusters can vary significantly from that in NGC 2808, as will be discussed later.

Our data do not provide sufficient time sampling to identify and characterize RR Lyrae stars. However, candidate RR Lyrae stars can be flagged by large exposure-to-exposure

photometric variations. In Figure 5, we have excluded candidate RR Lyrae stars by omitting stars that exhibit photometric variations that significantly exceed those of other stars at the same magnitude (at the level of 5σ or greater). A representative example of the photometric uncertainty is indicated by an error bar in the upper right-hand corner of each panel. Because the RR Lyrae instability strip is redder than the discontinuities we explore in this paper, the exclusions do not affect our analysis, but avoid cluttering the CCP with variable stars sampled at random phases.

Category 1: There are 9 clusters dominated by red clump stars (NGC 6366, NGC 6838, NGC 6496, NGC 6304, NGC 6652, NGC 6637, NGC 6352, NGC 5927, and NGC 6624). These clusters provide no information on any of the HB discontinuities.

Category 2: The HB distributions in 8 additional clusters (NGC 6121, NGC 6171, NGC 6584, NGC 5053, NGC 4590, NGC 6397, NGC 6101, and NGC 7099) extend through the RR Lyrae instability strip, but not far enough to populate the vicinities of the Grundahl and Momany jumps. Again, these clusters provide no information on the HB discontinuities.

Category 3: In 6 cases (NGC 6362, NGC 5466, NGC 6981, NGC 3201, NGC 1261, and NGC 362), there are less than four HB stars observed blueward of the G-jump, but those stars do in fact trace the deviations observed in the HB distribution of NGC 2808. In 4 of these clusters (NGC 362, NGC 5466, NGC 6981, and NGC 3201) there are a few blue-hook stars. However, given the scarcity of BHB and EHB stars, these clusters do not provide interesting constraints on the colors of the HB discontinuities.

Category 4: There are 16 clusters where the region between the Grundahl and Momany jumps is significantly populated, with few stars hotter than this region. All of the BHB stars trace the HB deviations observed in NGC 2808, and do so with enough stars to demonstrate consistency in the colors of the Grundahl and Momany jumps. In 9 cases (NGC 6717, NGC 6144, NGC 5024, NGC 6535, NGC 6934, NGC 6218, NGC 6341, NGC 288, and NGC 6779), there are no stars hotter than the M-jump. In 7 more clusters (NGC 5272, NGC 2298, NGC 6809, NGC 6723, NGC 5904, NGC 6254, and NGC 4833), those few stars hotter than the M-jump include blue-hook stars. Some of these clusters (e.g., NCC 5904, NGC 6779, NGC 6254, and NGC 4833), exhibit a sharp decline in the density of HB stars at the M-jump, but this is likely a coincidence, given that other clusters in this category (e.g., NGC 6341 and NGC 288) exhibit sharp declines unassociated with any particular HB discontinuity.

Category 5: There are 14 clusters (NGC 6681, NGC 6656, NGC 6441, NGC 5986, NGC 5286, NGC 6388, NGC 6541, NGC 6093, NGC 7089, NGC 6205, NGC 5139, NGC 7078, NGC 6715, and NGC 2808 itself) that have significant numbers of stars straddling both the Grundahl and Momany jumps. Most of these also host blue-hook stars, with the exception of NGC 6681, NGC 6656, NGC 6441[15], and NGC 6093, which truncate in the gap between the blue-hook stars and the normal EHB population. NGC 6656 (M22) looks somewhat unusual blueward of the M-jump, where the $C_{\rm F275W,F336W,F438W}$ index does not completely overlap with that of NGC 2808. In most of these 14 clusters, the HB discontinuities have the same $m_{F275W} - m_{F438W}$ colors as those in NGC 2808; the exceptions are NGC 6388 and NGC 6441, which each exhibit a G-jump that is significantly bluer than normal. The red clump distributions of NGC 6388 and NGC 6441 also appear very distinct from those in the other clusters, with NGC 6388 having a bifurcated structure (see also Bellini et al. 2013b).

[15] NGC 6441 hosts a population of subluminous HB stars that are much redder than the blue-hook stars found in other clusters, so their status is unclear (Brown et al. 2010).

Table 1
Survey Clusters with Blue-Hook Stars

NGC	$n_{\rm HB}$	$n_{\rm BH}$	NGC	$n_{\rm HB}$	$n_{\rm BH}$	NGC	$n_{\rm HB}$	$n_{\rm BH}$
362	303	2	5286	386	2	6541	228	3
2298	56	2	5466	30	1	6715	916	120
2808	757	52	5904	132	2	6723	150	1
3201	31	1	5986	328	3	6809	35	2
4833	138	1	6205	244	4	6981	64	1
5139	825	156	6254	86	1	7078	390	7
5272	179	1	6388	953	2	7089	515	3

4.2. *Clusters with Blue-Hook Stars*

Our sample includes 21 clusters with blue-hook stars, extending to 23 the tally of globular clusters known to host blue-hook stars. In Table 1, we list these clusters, along with the total number of HB stars in each sample ($n_{\rm HB}$), and the total number of blue-hook stars ($n_{\rm BH}$) that are blue enough to be unambiguously classified. Specifically, we classify them as blue-hook stars if they fall within $-2.4 \leq m_{\rm F275W} - m_{\rm F438W} \leq -1.9$ mag and $1.0 \leq C_{\rm F275W,F336W,F438W} \leq 1.3$ mag in the CCP after alignment with NGC 2808. Note that there are clusters in our sample where a few additional stars fall immediately to the red of this selection region, which might also be blue-hook stars, but their classification would not be secure (NGC 5139, NGC 5286, NGC 5986, NGC 6205, NGC 6254, NGC 6541, NGC 6715, NGC 6723, and NGC 7089).

To date, UV photometry had been used to confirm blue-hook stars in six globular clusters: NGC 5139 (ω Cen), NGC 2808, NGC 6715 (M54), NGC 2419, NGC 6388, and NGC 6273 (D'Cruz et al. 2000; Brown et al. 2001; Dalessandro et al. 2008; Dieball et al. 2009; Brown et al. 2010). Although our sample does not include NGC 2419 and NGC 6273, it does include the others, and the CCP of Figure 5 confirms the presence of blue-hook stars in each cluster. Dieball et al. (2009, 2010) provided four additional clusters that may host a small number of blue-hook stars each: NGC 6093 (M80), NGC 6681 (M70), NGC 7078 (M15), and NGC 6441. Of these clusters, three (NGC 6093, NGC 6441, and NGC 6681) do not however appear to host blue-hook stars in our sample, but NGC 7078 clearly does. We also find blue-hook stars in 16 additional clusters: NGC 362, NGC 2298, NGC 3201, NGC 4833, NGC 5272 (M3), NGC 5286, NGC 5466, NGC 5904 (M5), NGC 5986, NGC 6205 (M13), NGC 6254 (M10), NGC 6541, NGC 6723, NGC 6809 (M55), NGC 6981 (M72), and NGC 7089 (M2). In 7 of these clusters (NGC 3201, NGC 4833, NGC 5272, NGC 5466, NGC 6254, NGC 6723, and NGC 6981), there is only a single star falling unambiguously in the blue-hook region. The classification seems secure, given the placement in both the CMD and CCP, and the lack of other stars in the vicinity that would otherwise suggest significant contamination. In the 23 clusters hosting blue-hook stars, these stars comprise up to 20% of the HB population, although the percentage is highest in three of the most massive clusters

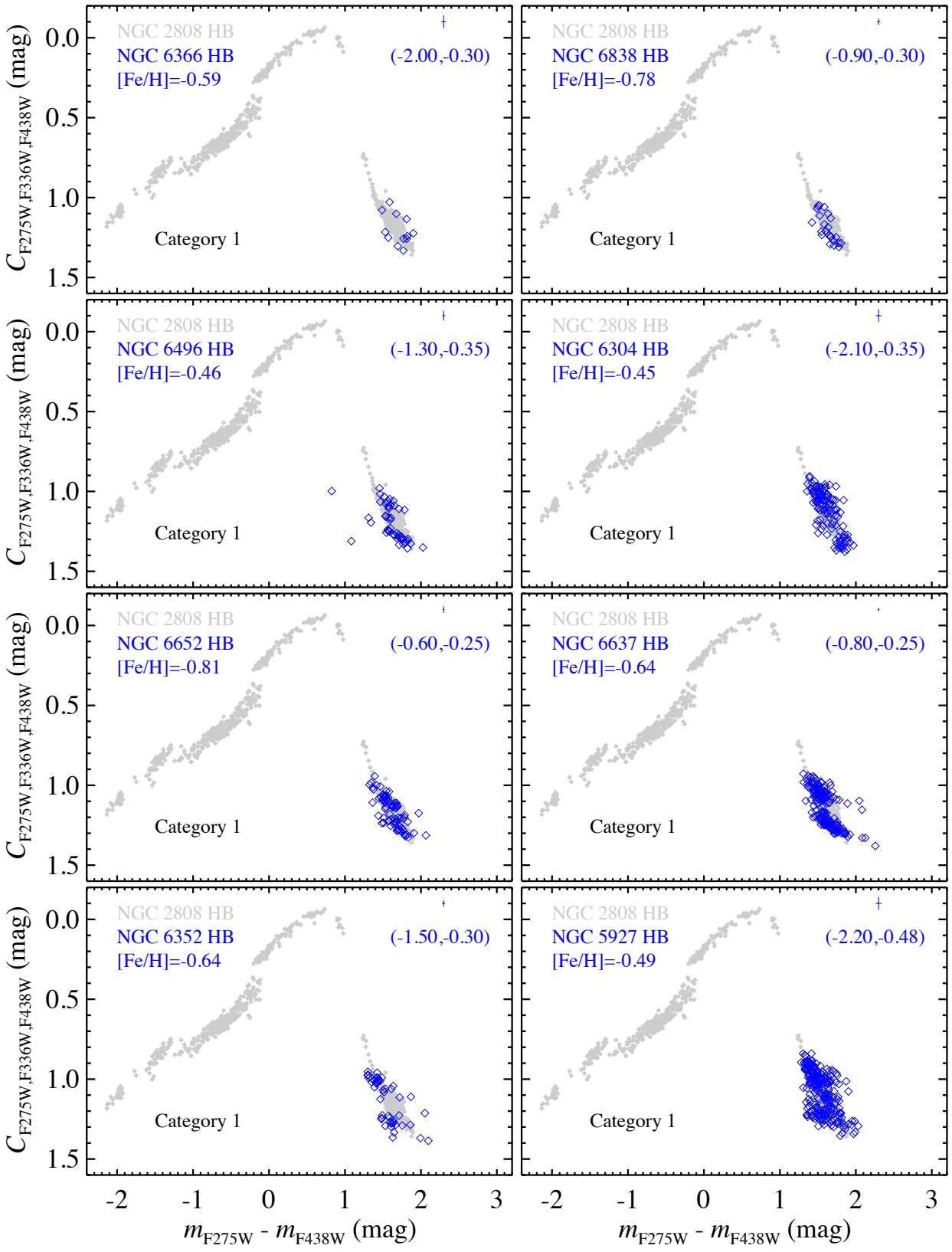

Figure 5. The HB distributions of each globular cluster in our sample (*blue points*) compared to that of NGC 2808 (*grey points*). The HB distribution of each cluster has been aligned with that of NGC 2808 at the C_{peak}, using the shifts indicated in parentheses. To aid comparisons, the clusters are sorted into arbitrary categories of increasingly blue HB morphology (see text). The metallicity of each cluster is indicated (Harris 1996; Brown et al. 2010). Representative photometric errors are shown (*error bar* in each panel). Candidate RR Lyrae stars have been excluded.

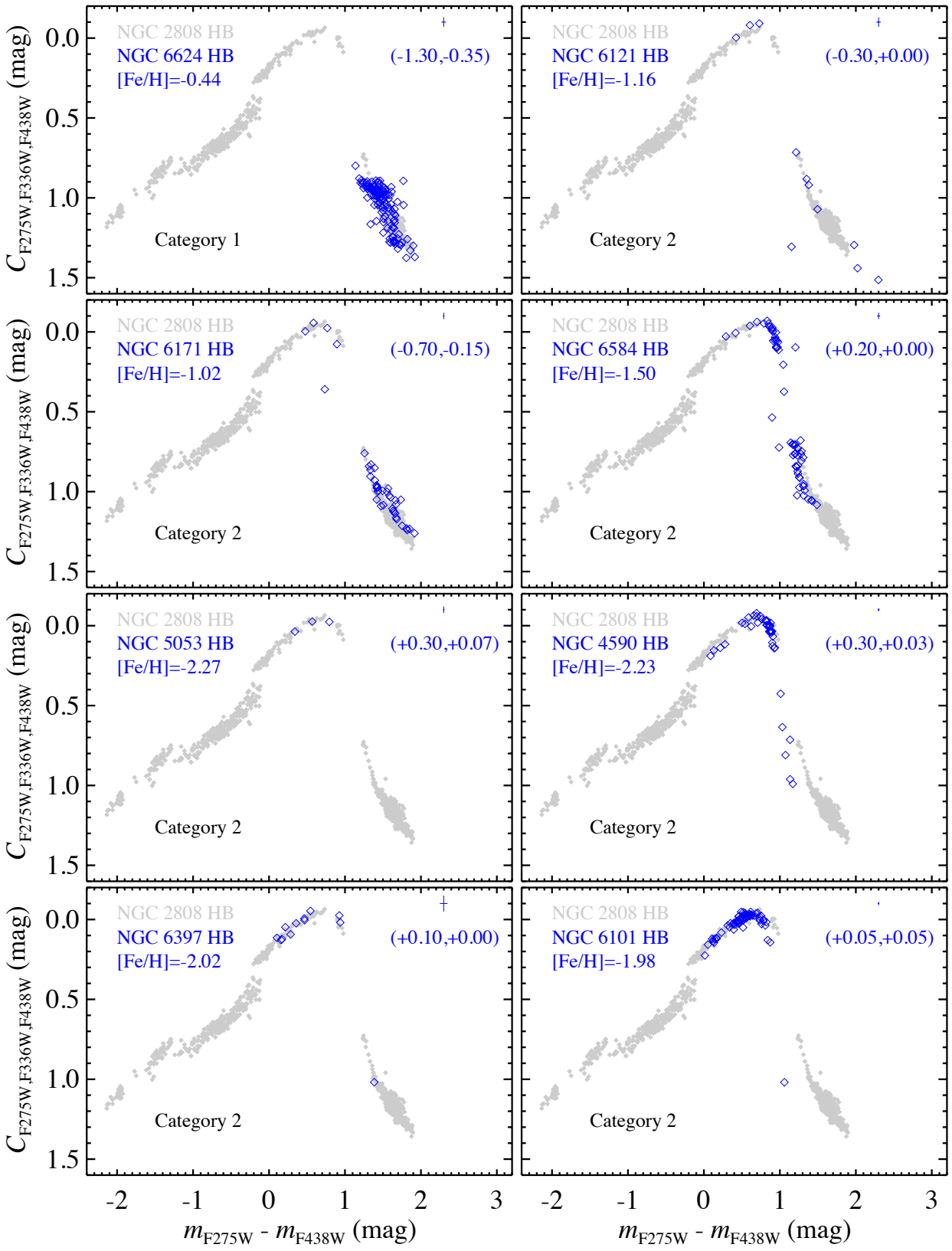

Figure 5. *Continued*

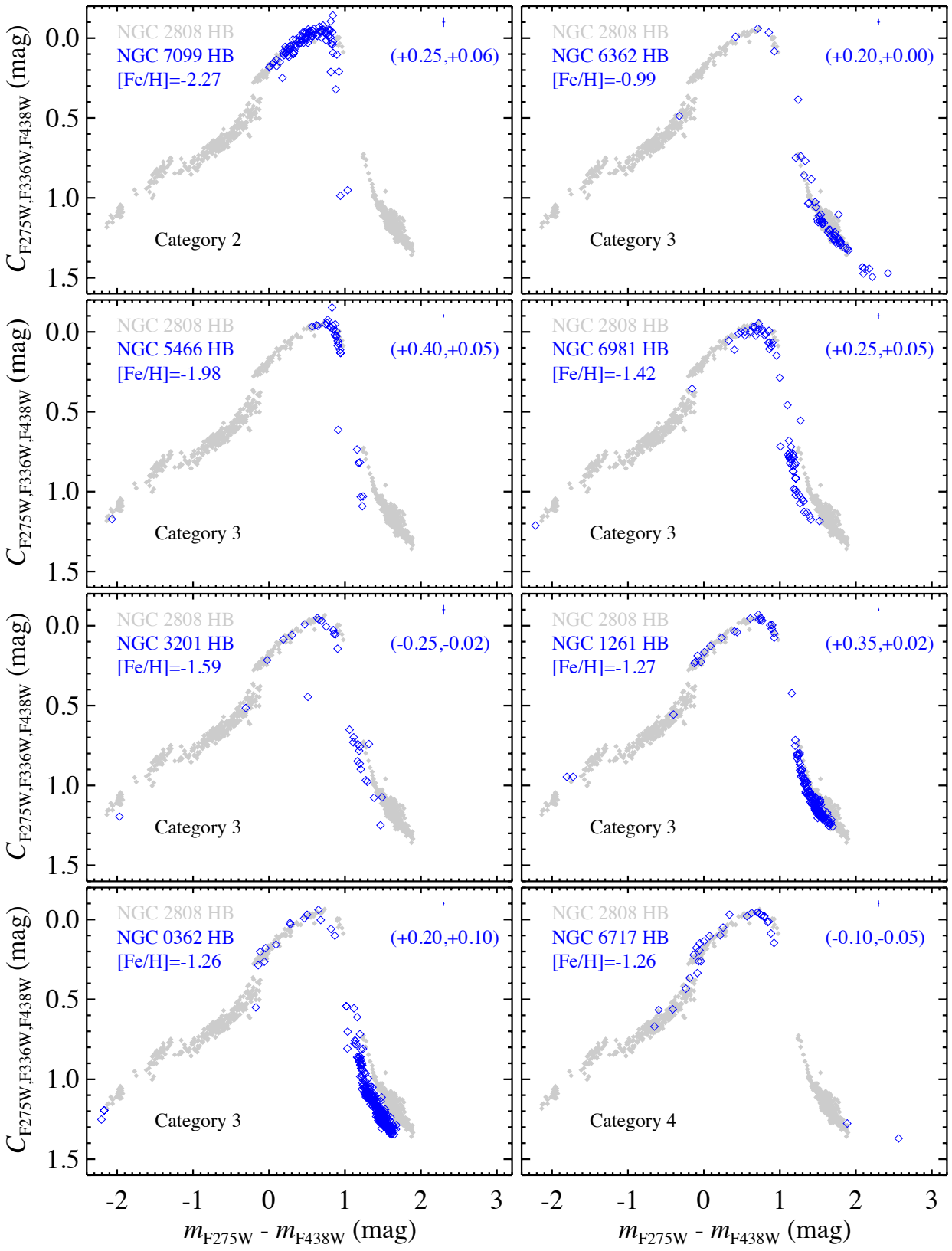

Figure 5. *Continued*

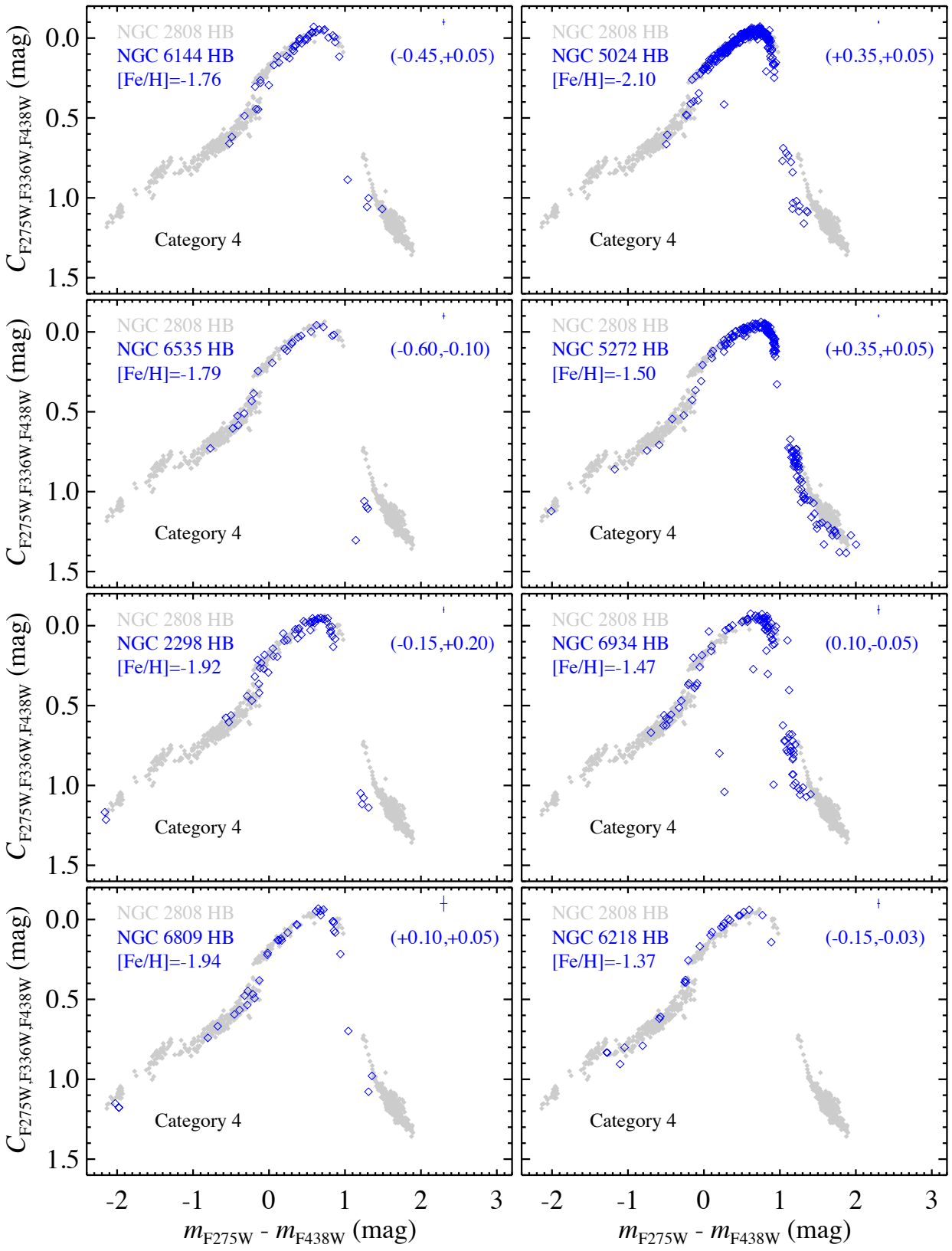

Figure 5. *Continued*

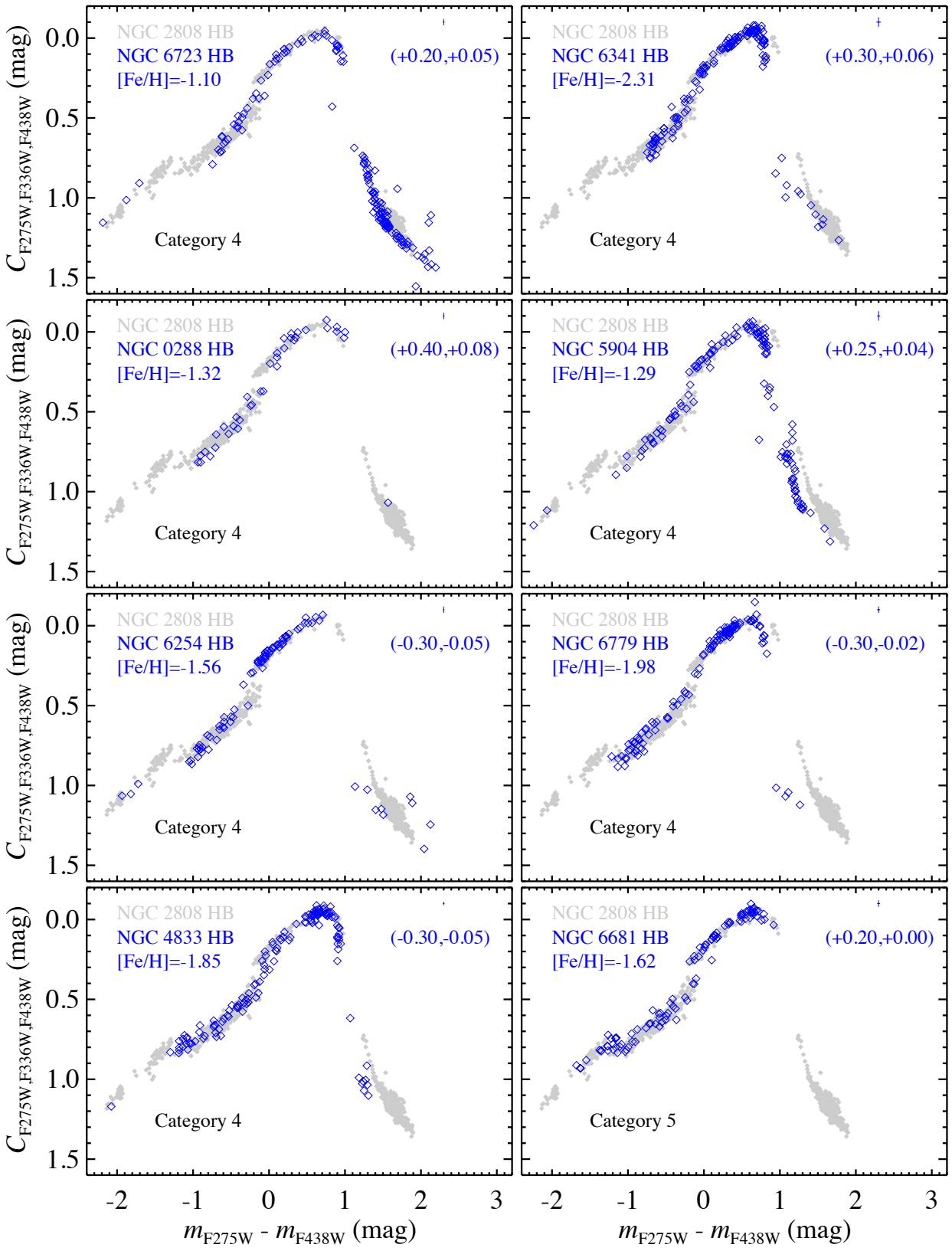

Figure 5. *Continued*

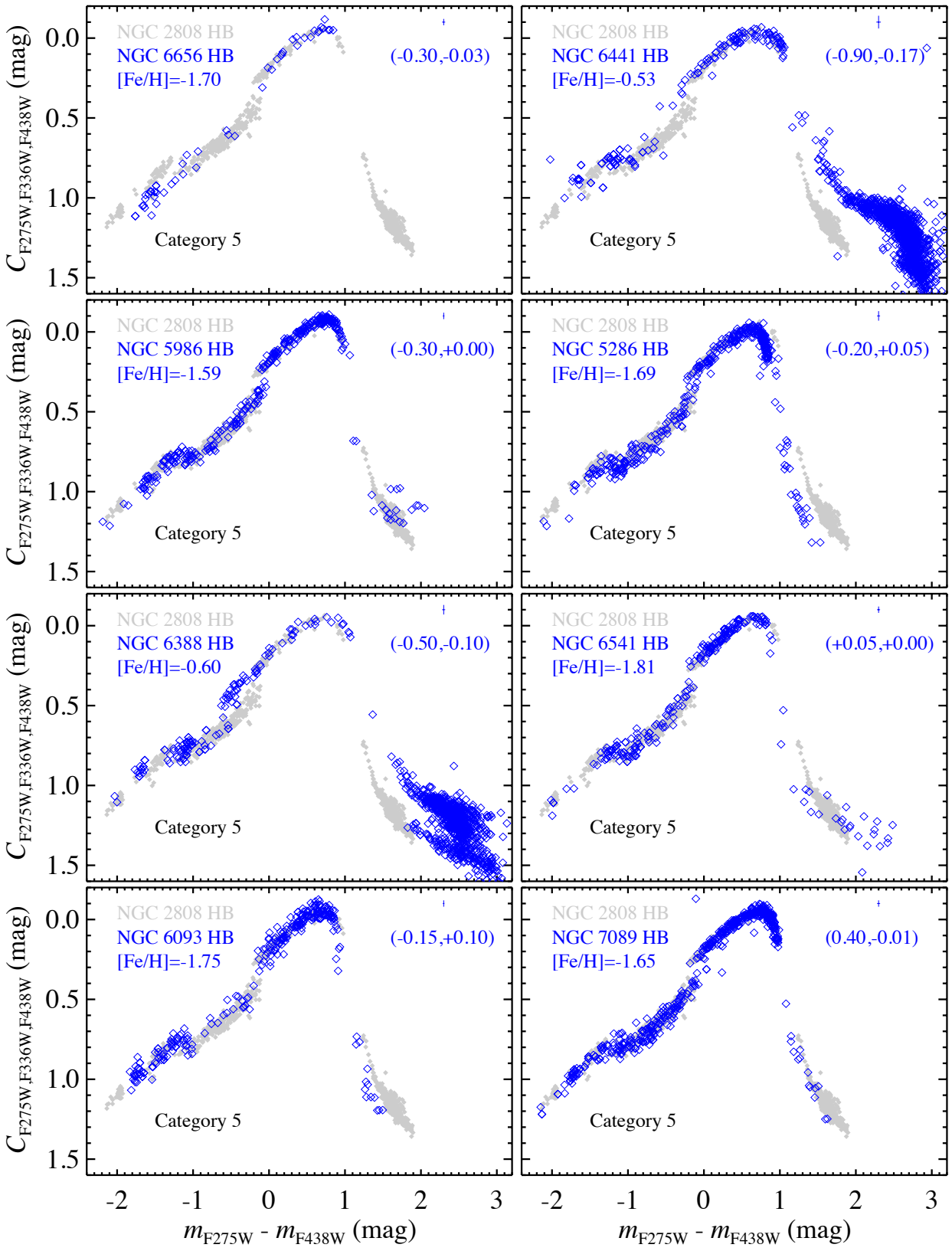

Figure 5. *Continued*

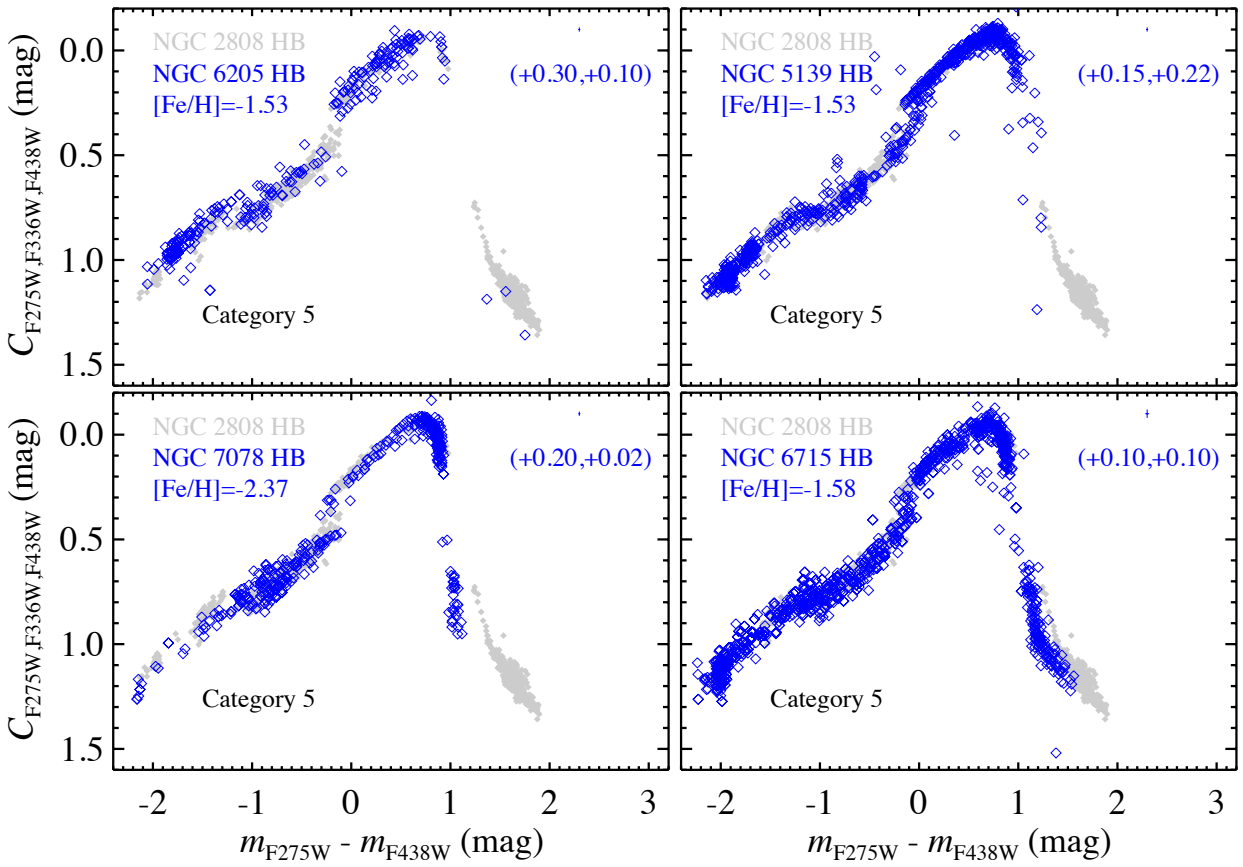

Figure 5. *Continued*

(NGC 2808, NGC 5139, and NGC 6715). Our sample of 53 clusters spans $-9.98 \leq M_V \leq -4.75$ mag in total luminosity (Harris 1996), with a median of −7.48 mag; 17 of the 21 clusters in our sample hosting blue-hook stars are in the brightest half of the sample, reinforcing the idea that blue-hook stars tend to form in the most massive clusters (see Brown et al. 2010 for a full discussion). For some of these clusters, the statistics are poor, with only one or two blue-hook stars, but we stress that the presence of blue-hook stars is not simply a matter of sampling enough stellar mass to find a relatively rare evolutionary phase. For example, the mean metallicities of NGC 5139 and NGC 5986 match within 0.1 dex, and the counts of their HB stars in our catalogs match within 3%, but NGC 5139, being the more massive cluster, has >20 times as many blue-hook stars as NGC 5986; this is another manifestation of parameters beyond metallicity affecting the HB morphology (i.e., the second-parameter problem).

4.3. *The Grundahl and Momany Jumps*

4.3.1. *NGC 6388 and NGC 6441*

In Figure 5, only two globular clusters exhibit significant discrepancies with the discontinuities of NGC 2808: NGC 6388 and NGC 6441. Specifically, in both of these clusters, the G-jump is ∼0.4 mag bluer than that observed elsewhere. In NGC 6388, the region between the G-jump and M-jump is well populated, such that the shift is obvious. In NGC 6441, the shift is less statistically significant, with only 6 stars falling blueward of the point where the G-jump occurs in NGC 2808, and only 2 of these stars at significantly bluer colors. That said, all 6 of these stars are well aligned with the $C_{F275W,F336W,F438W}$ trend extending from the cooler HB stars in NGC 6441, and over the $m_{F275W} - m_{F438W}$ color range of these 6 stars, there are no stars exhibiting a deviation from this trend (i.e., these 6 stars do not trace the locus of NGC 2808). In both NGC 6388 and NGC 6441, the shift in this feature implies that the onset for radiative levitation occurs at hotter effective temperature than the onset in other clusters, even after one accounts for the composition effects demonstrated in Figure 4.

To quantify this shift, in Figure 6 we compare the photometry of four clusters (NGC 2808, NGC 6715, NGC 6388, and NGC 6441) to theoretical ZAHB distributions from Brown et al. (2010). These ZAHB models assume that the HB stars evolved from MS stars with the standard chemical composition for each cluster (i.e., no He enhancement). The stellar structure models were then transferred to the observed CCP using the LTE synthetic spectra of Castelli & Kurucz (2003), applying the Fitzpatrick (1999) reddening law to provide appropriate SED-dependent extinction at each point along the ZAHB (thus avoiding the small approximation errors demonstrated in Figure 3), and subsequently folding the spectra through the WFC3 bandpasses. As in Figure 5, we aligned the theoretical distributions at the C_{peak}, using a least squares fit of the model to the data. The observed HB distribution (*black points*) between the Grundahl and Momany jumps clearly deviates from the theoretical distribution (*green curves*) in Figure 6; the model is shown as a dashed line over the region where the data deviate from the model. Over the range of the

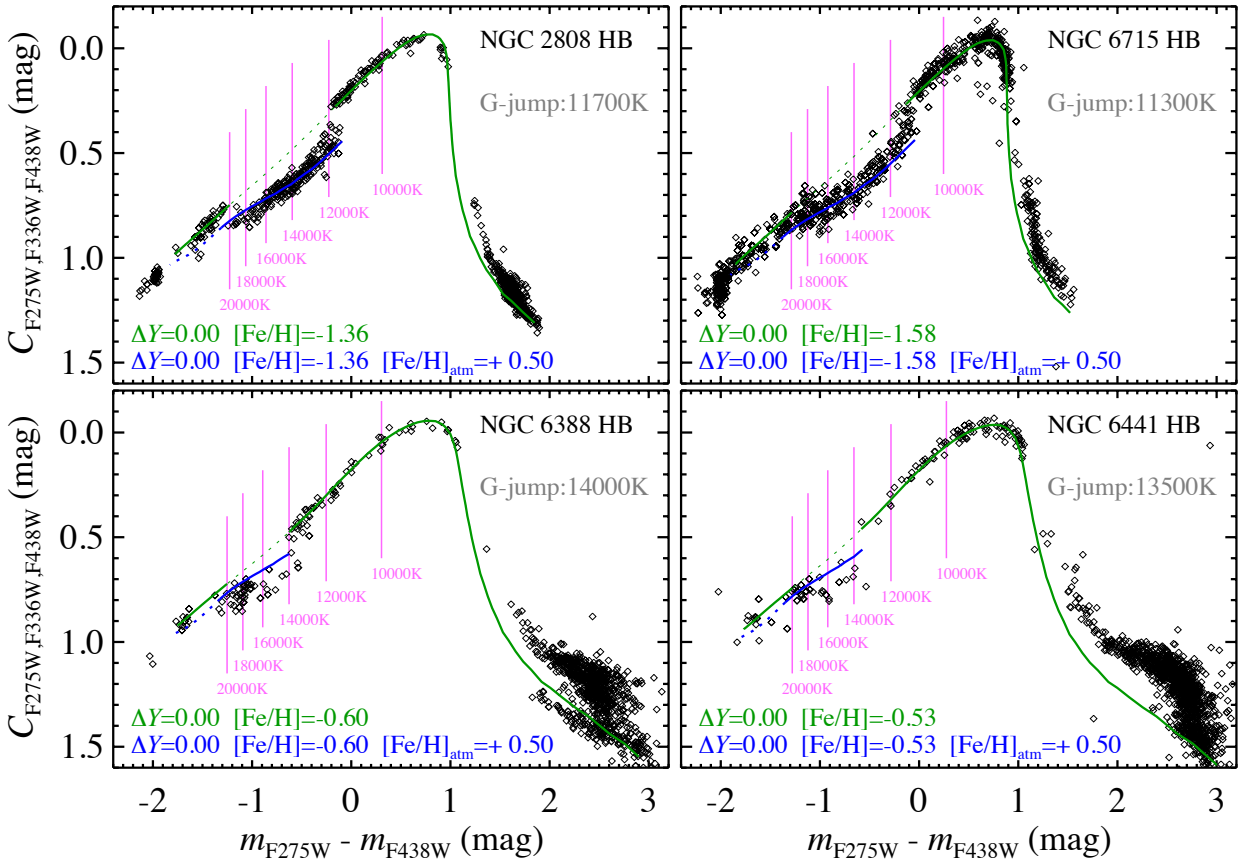

Figure 6. The HB distributions for 4 massive clusters in our sample (*black points*), compared to theoretical ZAHB distributions matching the cluster metallicity and assuming $\Delta Y = 0$ (*blue and green curves*). An effective temperature scale is shown to guide the eye (*pink lines*; labeled). If the ZAHB stellar structure models are transferred to the CCP using synthetic spectra representative of the cluster composition (*green curves*, shown as a *dotted line* between the G-jump and M-jump), the observed deviation between the Grundahl and Momany jumps is obvious. If the ZAHB stellar structure models are transferred to the CCP using synthetic spectra of enhanced metallicity (*blue curves*, shown as a *dotted line* beyond the M-jump), the model tracks the deviation between the G-jump and M-jump. Although the restoration of normal atmospheric abundances blueward of the M-jump matches the model to the data in this plane, this does not reproduce the behavior in the CMD (see Figure 8). We can use the points where the observed HB distribution deviates from the standard ZAHB distribution to determine the temperature of the G-jump and M-jump. For the intermediate-metallicity clusters NGC 2808 and NGC 6715 (*top panels*), the temperatures of those two features match those in dozens of other Galactic globular clusters (Figure 5). For the metal-rich clusters NGC 6388 and NGC 6441 (*bottom panels*), the G-jump is ∼2,000 K hotter than normal.

observed deviation, we also show the same stellar structure models, but transferred to the observable plane using synthetic spectra with an enhanced metallicity of [Fe/H] = 0.5 (the maximum metallicity available in the grid of synthetic spectra), simulating the effects of radiative levitation in the atmospheres (*blue curves*). For NGC 6388 and NGC 6441, the deviation observed between the G-jump and M-jump is more significant than that in the model. This may be due to the fact that the stars in these clusters were born at much higher metallicity than NGC 2808, such that a simulation of radiative levitation would require a metallicity exceeding [Fe/H] = 0.5. Of course, our use of [Fe/H] = 0.5 synthetic spectra is only a crude approximation of the actual interplay between gravitational settling and radiative levitation in the stellar atmospheres, which produces large element-to-element variations.

The effective temperatures for the G-jump and M-jump in each cluster are determined by observing where the observed HB distribution deviates from the ZAHB distribution transferred with synthetic spectra at standard cluster composition (*green curves*). Although the M-jump is well-defined in NGC 2808, it is spread over a significant color range in NGC 6715, NGC 6388, and NGC 6441. Nonetheless, a transition temperature of 20,000 K is consistent with the observed M-jump in each cluster. For NGC 2808 and NGC 6715, the temperature of the G-jump is close to the ∼11,500 K temperature reported at the time of its original discovery (Grundahl et al. 1998, 1999). In contrast, the G-jump occurs at ∼14,000 K in NGC 6388 and ∼13,500 K in NGC 6441, although given the small number of stars in the vicinity of the NGC 6441 G-jump, this value is uncertain at the level of a few hundred degrees.

Although the models in Figure 6 employ metallicities appropriate for each cluster, these clusters exhibit variations in He enhancement along the HB, and the assumed Y has a small but non-negligible effect on the alignment of the models to the data (see Figure 4). For this reason, in Figure 7 we also characterize the effective temperatures of the discontinuities using ZAHB models representing sub-populations with strong He enhancement ($\Delta Y = 0.17$). The temperature determinations shown in Figures 6 and 7 bracket the possibilities in each cluster. Even if one tries to minimize the temperature distinctions in the G-jump for each cluster, by assuming the coolest estimates for the metal-rich clusters (NGC 6388 and NGC 6441) and the hottest estimates for the clusters at lower metallicity

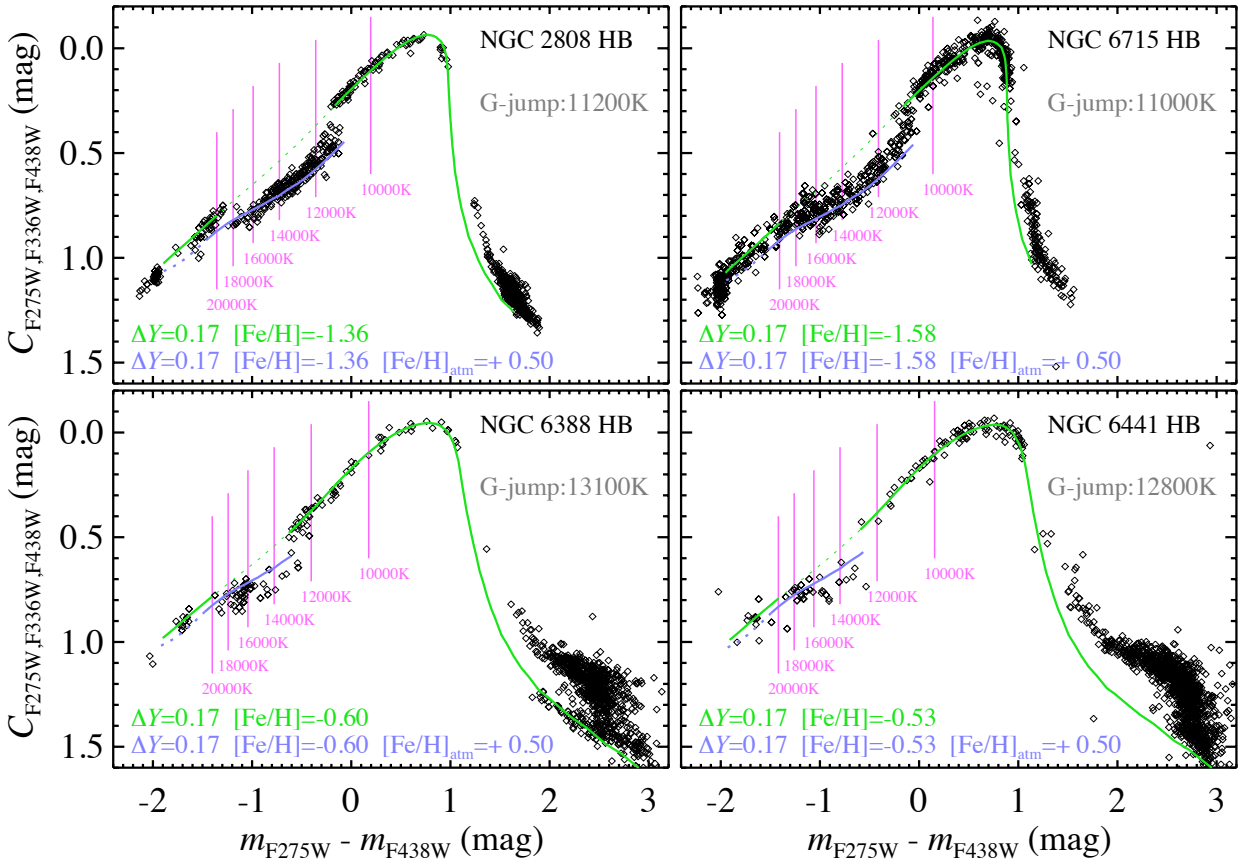

Figure 7. The same as Figure 6, but with He-enhanced stellar structure models. Although the stellar structure models are matched to each cluster in metallicity, the He abundance has a small but non-negligible effect on the alignment of the models to the data (see Figure 4). For this reason, the effective temperature of the G-jump and M-jump in each cluster is bracketed by the estimates here and those in Figure 6. The G-jump in the metal-rich clusters (NGC 6388 and NGC 6441) is much hotter than that in the other clusters, even if one takes the coolest estimate (here) for the metal-rich clusters and the hottest estimate (Figure 6) for the other clusters.

(NGC 2808 and NGC 6715), the metal-rich clusters have G-jump temperatures at least 1,100 K hotter than those in the other clusters.

4.3.2. *Caveats*

Figures 6 and 7 simulate the effects of radiative levitation in BHB stars by assuming a super-solar metallicity between the G-jump and M-jump. The evidence for radiative levitation blueward of the G-jump is well supported by spectroscopy of BHB stars (e.g., Moehler et al. 1999, 2000; Behr 2003; Pace et al. 2006). In the CCP, the observed HB locus returns to alignment with the standard ZAHB distribution (i.e., with no atmospheric enhancement of metallicity) blueward of the M-jump, but the complete cessation of radiative levitation cannot be the origin of the M-jump; instead, some other effect is likely counterbalancing the deviation associated with radiative levitation. There are few metallicity measurements in globular clusters for EHB stars (i.e., at $T_{\rm eff} \gtrsim 20,000$ K), although Brown et al. (2012) found that some (but not all) of these stars in NGC 2808 exhibited super-solar Fe abundances. The sdB stars of the Galactic field population are the analogs of the EHB stars in globular clusters, and Geier et al. (2010) found that the Fe enhancement in sdB stars hotter than 20,000 K is similar to that in the BHB population of globular clusters. Furthermore, blueward of the G-jump, the enhancement of atmospheric metals is accompanied by a corresponding depletion in atmospheric He. In ω Cen, this He depletion continues at temperatures well past 20,000 K; in fact, the depletion continues until $T_{\rm eff} > 32,000$ K, where the blue-hook stars exhibit atmospheres greatly enhanced in He (Moehler et al. 2011). A similar result was found in NGC 6752, with surface He significantly depleted over the entire range of 12,000 K – 32,000 K (Moni Bidin et al. 2007).

Besides this evidence, we can demonstrate with our own data that the M-jump cannot be induced by the restoration of normal atmospheric abundances at temperatures above 20,000 K. In Figure 8, we show the same data and models that appeared in Figures 6 and 7, but now the ordinate uses m_{F336W}, similar to the U band employed by Grundahl et al. (1999) and Momany et al. (2002) in their CMDs characterizing the G-jump and M-jump. As noted previously, the use of [Fe/H] = 0.5 spectra is a crude approximate for the abundance variations incurred through atmospheric diffusion, and the HB exhibits a range of Y values at any particular color, due to dispersions in RGB mass loss. It is impossible to disentangle these complexities using broad-band photometry. However, the purpose of the comparison here is to demonstrate the qualitative effects of radiative levitation in the atmosphere (and the effects of He abundance in the stellar structure models, which will be discussed below). The onset of radiative levitation blueward of $m_{F275W} - m_{F438W} = -0.2$ mag causes an upward jump in the m_{F336W} photometry, such that

the sense of the shift is the same in the model and the data. However, the cessation of radiative levitation blueward of $m_{F275W} - m_{F438W} = -1.2$ mag causes a downward shift in the model, in contrast to the data. Thus, the onset of radiative levitation explains the G-jump in both the CCP (Figures 6 and 7) and the CMD (Figure 8), but the cessation of radiative levitation does not simultaneously reproduce the behavior of the M-jump in both diagrams.

Although a discussion of the red clump morphology in these clusters is beyond the scope of the current paper, we note some clusters exhibit red clump distributions in the CCP (Figure 5) that are distinct from that of NGC 2808. The distinction can be modest (e.g., NGC 5286 and NGC 5904) or severe (e.g., NGC 6388 and NGC 6441), and is likely driven by metallicity effects in the reddest HB stars. However, even if we calculate ZAHB distributions at the appropriate metallicity for NGC 6388 and NGC 6441, there is a significant mismatch between the models and data in Figures 6 and 7. These stars are as cool as those on the MS, where the sensitivity of the $C_{F275W,F336W,F438W}$ index to CNO abundances makes it a useful diagnostic in the exploration of multiple populations (see Milone et al. 2012). The distortions of the red clump here may be related to the distinct MS morphologies of these two metal-rich clusters. Bellini et al. (2013b) demonstrated that the MS of NGC 6441 is clearly split into two branches, while that of NGC 6388 is broadened but not split. They hypothesized that the second generation of stars in each cluster has a similarly enhanced He abundance but distinct CNO abundances. Those CNO variations may explain why the two clusters exhibit distinct red clump morphologies in Figures 6 and 7. The predicted morphology of HB evolutionary tracks with CNO-enhanced mixtures (Pietrinferni et al. 2009) seems to be consistent with this possibility (see also the optical analysis of NGC 1851 by Gratton et al. 2012).

4.3.3. *Origin of the G-jump and M-jump*

The G-jump is associated with a sharp increase in atmospheric metallicity, decrease in atmospheric He, and decrease in stellar rotation. We can now add that the G-jump is almost universally consistent in effective temperature, with the notable exceptions of NGC 6388 and NGC 6441. The most likely reason for the increased temperature of the G-jump in NGC 6388 and NGC 6441 is that the BHB stars in these two metal-rich clusters are significantly enhanced in He, compared to BHB stars in relatively metal-poor clusters; at higher metallicities, a larger He abundance is needed to populate the BHB. As mentioned previously, all globular clusters appear to exhibit sub-populations with distinct chemical compositions, but the phenomenon is strongest in massive globular clusters, where there exist sub-populations enhanced in He up to $Y \sim 0.4$ ($\Delta Y \sim 0.17$; see Piotto et al. 2015 and references therein).

At a fixed age, the MS turnoff mass decreases as He increases, and thus for a given amount of RGB mass loss, MS stars at higher Y tend to produce HB stars of lower mass and higher effective temperature. He enhancement also affects the HB luminosity. On the red clump and BHB, He-enhanced stars are brighter than normal, due to the larger energy output of their hydrogen shells that results from their lower envelope opacity and higher envelope mean molecular weight (see, e.g., Sweigart 1987). In contrast, on the EHB, He-enhanced stars are fainter than normal, since they have smaller He core masses (see, e.g., Sweigart & Gross 1978) and insufficient envelope masses to support an active hydrogen shell (Valcarce et al. 2012). NGC 2808 is an instructive example for these effects. From the first parameter of HB morphology (metallicity), one might expect an HB distribution that does not extend to the end of the EHB, given its intermediate metallicity ([Fe/H] = −1.36; Walker 1999)[16]. However, we know that massive clusters tend to host significant EHB populations associated with He-enriched populations (see Milone et al. 2014). This is true in NGC 2808 ($M_V = -9.4$ mag; Harris 1996), which hosts sub-populations with varying amounts of He enhancement (up to $Y \sim 0.4$; D'Antona et al. 2005; Piotto et al 2007); its hotter HB stars are generally drawn from sub-populations with higher Y, with increasingly large deviations from the luminosity of the canonical HB (e.g., D'Antona & Caloi 2004; Brown et al. 2010; Dalessandro et al. 2011). In the atmospheres of its BHB stars, Marino et al. (2014) also found that He is enhanced, until the point of the Grundahl jump, where He is depleted through gravitational settling. The varying progenitor populations for HB stars as a function of color is reinforced by the work of Gratton et al. (2011), who found that the BHB stars in NGC 2808 are O-poor and Na-rich (corresponding to the blue sub-population on the MS), while its red HB stars are O-rich and Na-poor (corresponding to the red sub-population on the MS). Another example of these effects can be seen in the comparison of M3 and M13, two intermediate-metallicity clusters with distinct HB morphology that can be traced to He enhancement ($\Delta Y \sim 0.02$–0.04) in M13 (Dalessandro et al. 2013).

Along similar lines, the metallicities of NGC 6388 ([Fe/H] = −0.60; Piotto et al. 2002) and NGC 6441 ([Fe/H] = −0.53; Harris 1996) are so high[17] that they would normally produce an HB falling entirely in the red clump. However, the HB morphology of each cluster extends far to the blue (Rich et al. 1997), including significant populations of unusually-bright RR Lyrae stars (Layden et al. 1999; Pritzl et al. 2001, 2002, 2003; Corwin et al. 2006) that belong to neither Oosterhoff class (Pritzl et al. 2000). The HB of each cluster is over-luminous blueward of the red clump, implying that the BHB stars originate in a MS population enhanced to $Y \sim 0.4$ (or equivalently $\Delta Y \sim 0.14$–0.17; Busso et al. 2007; Caloi & D'Antona 2007; D'Antona & Caloi 2008; Brown et al. 2010). He enhancement is required to move a metal-rich HB star blueward from the red clump to the BHB while increasing its luminosity.

To demonstrate the effects of Y enhancement on HB luminosity, we show in Figure 8 the same HB distributions of Figures 6 and 7, but using CMDs with m_{F336W} (U) on the ordinate. To ease comparisons between the clusters, the observed HB distributions are again aligned to that of NGC 2808 (with the same color alignment employed in previous figures). Here, the theoretical ZAHB distributions (Brown et al. 2010) have been calculated for stars at $\Delta Y = 0.0$ (*dark green*; the same models in Figure 6) and $\Delta Y = 0.17$ (*light green*; the same models in Figure 7). As in Figures 6 and 7, the radiative levitation of metals is simulated through the use of super-solar spectra (*blue*). The abscissa alignment of the models to the data is the same as that used in Figures 6 and 7, while the ordinate alignment of the models to the data places the ZAHB

[16] The Walker et al. (1999) metallicity is on the Zinn & West (1984) metallicity scale. Recently, Carretta (2015) found [Fe/H] = $-1.129 \pm 0.005 \pm 0.034$ on the UVES scale, but the distinction makes no difference in our analysis here.

[17] Note that Carretta et al. (2009) find NGC 6388 and NGC 6441 to be at [Fe/H] = -0.45 ± 0.04 and -0.44 ± 0.07, respectively, on the UVES scale, but as with NGC 2808, the distinction makes no difference to our analysis here.

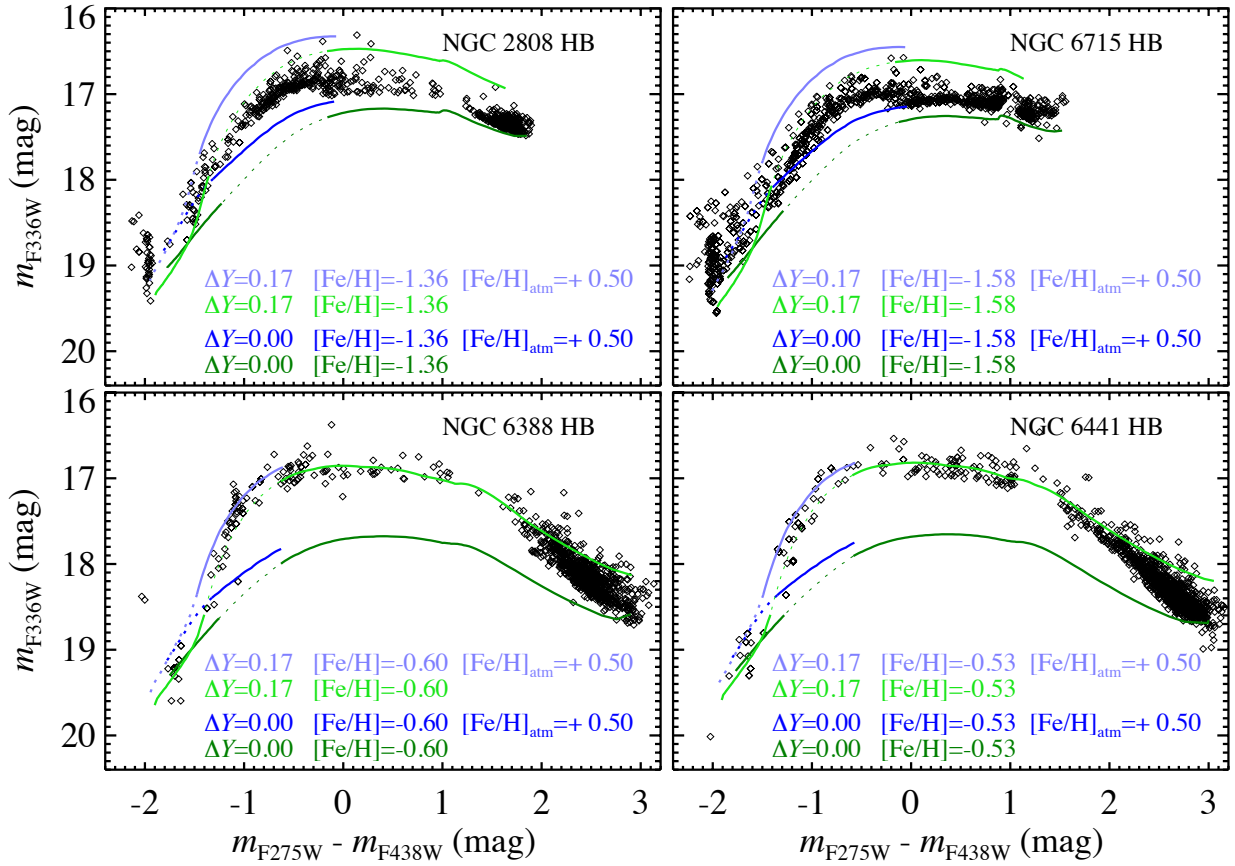

Figure 8. The same data and models shown in Figures 6 and 7, but the ordinate has been replaced with m_{F336W} (U). Although the G-jump and M-jump were each discovered in CMDs of U vs. color, these discontinuities are more obvious in the CCP than they are in the CMD here. The theoretical ZAHB distributions were normalized in luminosity such that the $\Delta Y = 0$ model aligns with the base of the red clump, while the color alignment is the same as that shown in Figures 6 and 7. With broad-band photometry, it is impossible to disentangle the effects of He enhancement (accounted in the stellar structure models) and the radiative levitation of metals (accounted in the synthetic spectra used to transfer them to the observable plane), but the purpose here is to demonstrate qualitatively these effects in the CMD. The onset of radiative levitation for stars hotter than the G-jump causes an upward shift in both the model (via synthetic spectra with super-solar abundances) and the data. The cessation of radiative levitation for stars hotter than the M-jump causes a downward shift in the model, in contrast to the data, which exhibit an upward shift. Thus, the complete cessation of radiative levitation on the EHB does not explain the M-jump, even though it reproduces the behavior in the CCP (Figures 6 and 7). Redward of the G-jump, the observed HB luminosity in NGC 6715 is close to that of the $\Delta Y = 0$ model, indicating little He enhancement of its BHB stars, while the luminosity in NGC 2808 falls between the $\Delta Y = 0$ and $\Delta Y = 0.17$ models, consistent with a moderate He enhancement. In contrast, the BHB stars in NGC 6388 and NGC 6441 are much brighter than the ZAHB with no He enhancement ($\Delta Y = 0$), but consistent with the ZAHB representing strong He enhancement (ΔY =0.17). The hotter G-jump in NGC 6388 and NGC 6441 (see Figures 6) is likely due to the fact that their BHB stars were born at greatly enhanced He abundance. The G-jump is more difficult to discern in this CMD than in the CCP (compare with Figures 6), but it is still apparent in each cluster. In NGC 6388, there may be multiple deviations in the vicinity of the G-jump, near $m_{F275W} - m_{F438} \approx -0.6$ mag (also evident in Figure 6) and $m_{F275W} - m_{F438} \approx -0.3$ mag (closer to the usual temperature of the G-jump).

model with $\Delta Y = 0.0$ at the base of the observed red clump (on the assumption that the faintest red clump stars arise from a population unenhanced in He). In NGC 6715, the G-jump is clearly visible, but to the red of the G-jump, the observed HB stars are closer to the model for stars at $\Delta Y = 0.0$, implying that HB stars in the vicinity of the G-jump were born with little He enhancement. In NGC 2808, the G-jump is again clearly visible, but to the red of the G-jump, there is a more significant luminosity difference between the observations and the model for stars at $\Delta Y = 0.0$, implying that the HB stars in the vicinity of the G-jump were born with some He enhancement. For reference, D'Antona & Caloi (2004) used photometry to estimate that these stars have moderate enhancement, with $\Delta Y \sim 0.04$–0.06 (see also Dalessandro et al. 2011), while Marino et al. (2014) used spectroscopy to measure a He enhancement of $\Delta Y = 0.09 \pm 0.01 \pm 0.05$ (internal plus systematic uncertainty). For NGC 6388 and NGC 6441, the HB stars near the G-jump are much more luminous than the model for $\Delta Y = 0.0$, and nearly as bright as the model for $\Delta Y = 0.17$. This is in agreement with previous photometric results (e.g., Busso et al. 2007; Caloi & D'Antona 2007; D'Antona & Caloi 2008; Brown et al. 2010; Bellini et al. 2013b). Furthermore, the G-jump appears more complicated for these two clusters. For NGC 6441, the paucity of stars in the vicinity of the G-jump makes the jump difficult to discern (at least compared to the clear deviation in Figures 6 and 7). For NGC 6388, however, there appears to be a pair of jumps: one at the usual temperature for the G-jump (i.e., near 11,500 K), and a hotter one (i.e., near 14,000 K, corresponding to the obvious deviation in Figures 6 and 7); these appear as excursions from the dominant stellar locus.

If the BHB stars of NGC 6388 and NGC 6441 were born with a large He enhancement, can this explain the increased temperature for the G-jump in these clusters? To investigate this point, we show in Figure 9 the behavior of the convective zones due to H, He I, and He II ionization near the sur-

face of HB stars, as a function of effective temperature, using evolutionary models calculated at metallicities appropriate for NGC 6388 and NGC 2808. The figure shows the convective zones for HB stars with $\Delta Y = 0.03$ (*red shading*) and $\Delta Y = 0.17$ (*blue shading*). Sweigart (2002) and Cassisi & Salaris (2013) used similar figures (with no He enhancement) to demonstrate how the surface convection from the He I ionization zone disappears at temperatures hotter than ∼12,000 K, enabling the onset of radiative levitation in BHB stars and the appearance of the G-jump. Here, we show the convection zones for two different Y assumptions, demonstrating that the He I convection is sensitive to initial Y, while the He II and H convection zones are not. Comparing the convective zones in the top (intermediate metallicity) and bottom (high metallicity) panels, it is clear that Y (and not [Fe/H]) is the critical parameter governing the behavior of the He I convection zone, and thus the G-jump, although we note that there are other changes in the convection zones that depend upon [Fe/H]. Specifically, increasing [Fe/H] shifts the termination of the H convection zone hotter by 500–1000 K (depending upon Y) and extends the tail of the He II convection zone to both hotter temperatures and shallower depths.

With this behavior in mind, the convection zones in the vicinity of the G-jump (from H and from He I) offer two possible explanations for the G-jump. Qualitatively, a convective zone acts as a fully mixed reservoir of matter having the original chemical composition, which minimizes the effects of diffusion (gravitational settling and radiative levitation). The G-jump could be due to the He I ionization, as hypothesized by Sweigart (2002) and Cassisi & Salaris (2013). In this view, the BHB stars in most clusters are born with little to modest He enhancement, such that there is little variation in the effective temperature of the G-jump. In NGC 6388 and NGC 6441, the BHB stars have a significant enhancement near $\Delta Y \sim 0.17$; along the HB, this shifts the cessation of He I ionization to hotter effective temperatures by ∼2,000 K – the same shift observed. In this scenario, it is unclear if the G-jump in NGC 2808 (with stars near $\Delta Y \sim 0.09$) would be so similar to the G-jump in less massive clusters that exhibit little He enhancement in their sub-populations (see Figure 5). Alternatively, the G-jump in most clusters could be due to the H convection zone. In this view, the G-jump remains at constant effective temperature in most clusters because the H convection is insensitive to Y. However, for BHB stars with He abundances near $\Delta Y \sim 0.17$, the He I ionization shifts to hotter effective temperature and moves closer to the stellar surface. This would make the G-jump appear at hotter effective temperature (as in Figure 5) if it arises from He I convection, or even multiple temperatures (as might be implied by Figure 8) if it arises from both H and He I convection. With both of these scenarios, the temperatures observed for the G-jump do not exactly coincide with the transitions in the modeled convection zones, even if the behavior is qualitatively consistent. It is likely the case that other parameters, such as turbulence, play a role in the exact location of the jumps; the region that is mixed at the surface may not coincide with the formal convective boundary. Along these lines, we note that Michaud et al. (2011) reproduce the G-jump at 11,500 K by invoking a fully mixed region near the surface of the star, with a mass $10^{-7}\ M_{\odot}$, possibly driven by turbulence or mass loss.

Another complication concerns the direction of the HB evolution beyond the ZAHB. As known since the work of Sweigart & Gross (1976), BHB stars with normal He abundances can slowly evolve redward toward cooler effective

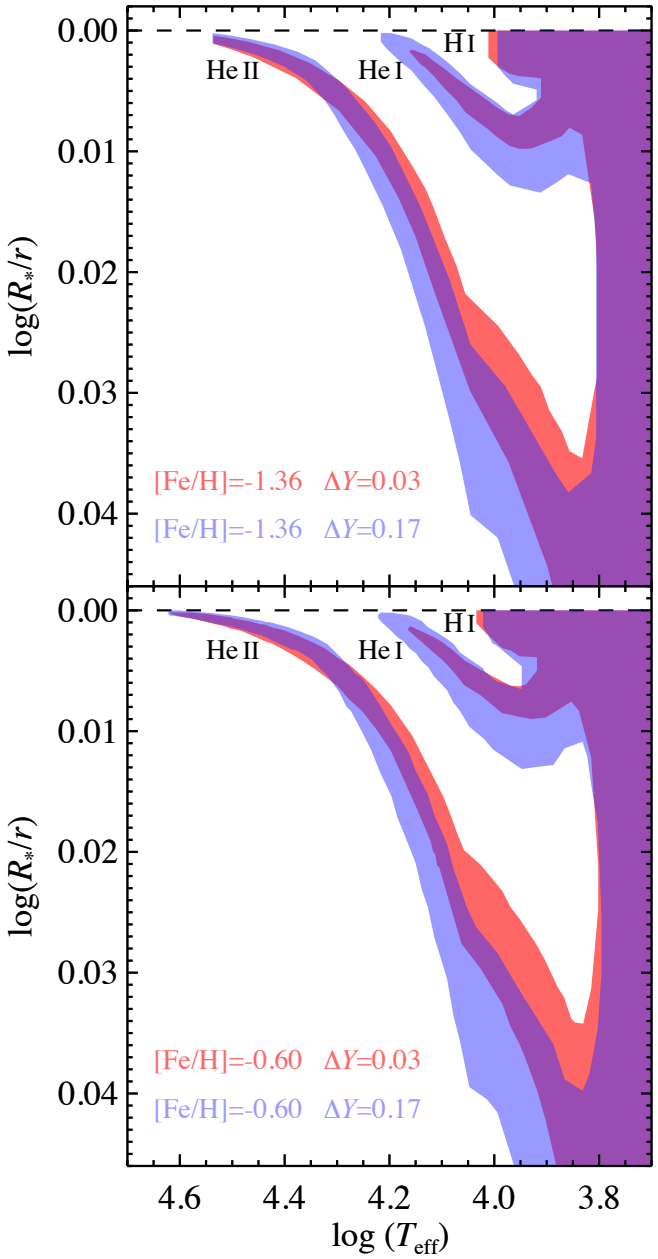

Figure 9. The location of the convection zones (*shading*) in ZAHB stars as a function of effective temperature, relative to the stellar surface (*dashed line*), assuming the metallicity of NGC 2808 (*top panel*) and NGC 6388 (*bottom panel*). When the He abundance is increased from $\Delta Y = 0.03$ (*red shading*) to $\Delta Y = 0.17$ (*blue shading*), the transition in the He I convective zone shifts to higher effective temperature by ∼2,000 K, and the He I convective zone moves closer to the surface. If the G-jump is normally associated with the He I convective zone, this temperature shift at high Y may explain the bluer G-jump in NGC 6388 and NGC 6441. If the G-jump is normally associated with the H convective zone, the surface encroachment of the He I convective zone at high Y may also explain the bluer G-jump in NGC 6388 and NGC 6441. Note that evolutionary effects, turbulence, and mass loss complicate this interpretation; these models only serve to provide possible explanations for the observed G-jump behavior in a qualitative sense. Similarly, if the M-jump is associated with the He II convective zone, the observed consistency of the M-jump temperature (even in NGC 6388 and NGC 6441) might be due to the insensitivity of the He II convective zone to Y.

temperatures, especially at low to intermediate metallicities. However, when their He enhancement is $\Delta Y = 0.17$, the HB stars in the vicinity of the G-jump can rapidly evolve blueward from temperatures cooler than 11,500 K to temperatures near

15,000 K. Depending upon the relative timescales of the various factors at work (surface convection, turbulence, mass loss, radiative levitation, gravitational settling), the distinct evolutionary paths for high-Y stars may also push the G-jump toward higher effective temperatures in clusters like NGC 6388 and NGC 6441. An exploration of these effects is currently underway (Tailo et al., in prep.).

As noted previously, the M-jump cannot be due to a simple disruption of radiative levitation at temperatures hotter than 20,000 K. Looking at Figure 9, it is worth noting that the He II convection zone begins to encroach upon the surface near this temperature, and the behavior is independent of He abundance. It may be a coincidence that the M-jump is also independent of He abundance, even in the two clusters exhibiting a hotter G-jump (NGC 6388 and NGC 6441), but we speculate that the M-jump may be associated with the He II convection zone.

5. SUMMARY

Using UV and blue photometry for 53 Galactic globular clusters, we have shown that the discontinuities in their HB distributions are remarkably consistent. Globular clusters are now known to host complex populations with variations in chemical composition, but these HB discontinuities reflect universal transitions in atmospheric phenomena, and not abundance distinctions in their MS progenitors. That said, the effective temperature for one of these discontinuities, the G-jump, is $\sim$1,000–2,000 K hotter in NGC 6388 and NGC 6441. This shift is likely due to the fact that these two clusters host BHB stars greatly enhanced in He ($\Delta Y \sim 0.17$), which affects the behavior of the He I convective zone and its role in disrupting radiative levitation.

Although the complexity of globular cluster populations was originally recognized in the most massive globular clusters, its ubiquity became more apparent with appropriate photometry. The history of blue-hook stars is following a similar path. This is not because massive clusters provide more chances to find a star following a relatively rare evolutionary avenue; instead, these clusters host sub-populations significantly enhanced in He, which leads to a hotter HB morphology. While blue-hook stars comprise a tiny fraction of the population in any globular cluster, we have shown that these products of extreme mass loss can be found in most of the bright globular clusters. The census of clusters hosting blue-hook stars has increased to 23, with nearly all of them residing in the brighter half of the Galaxy's globular cluster system.

Support for program GO-13297 was provided by NASA through a grant from the Space Telescope Science Institute, which is operated by the Association of Universities for Research in Astronomy, Inc., under NASA contract NAS 5-26555. S.C. and G.P. recognize partial support by the IAC (grant P301031) and the Ministry of Competitiveness and Innovation of Spain (grant AYA2010-16717); S.C., G.P., and F.D. recognize partial support by PRIN-INAF 2014 (PI: S. Cassisi). S.O. and G.P. also acknowledge partial support by the Università degli Studi di Padova Progetto di Ateneo CPDA141214 "Towards understanding complex star formation in Galactic globular clusters." A.P.M. acknowledges support by the Australian Research Council through Discovery Project grant DP120100475. F.R.F. and E.D. acknowledge the support from the Cosmic-Lab project (web site: http://www.cosmic-lab.eu) funded by the European Research Council, under contract ERC-2010-AdG- 267675. A.P. acknowledges support from PRIN-INAF2012 (PI: L. Bedin). S.O. gives thanks for the support of the University of Padova.

REFERENCES

Anderson, J. 1997, PhD thesis, Univ. California at Berkeley, Berkeley
Anderson, J., & Bedin, L.R. 2010, PASP, 122, 1035
Bedin, L.R., Piotto, G., Anderson, J., Cassisi, S., King, I.R., Momany, Y., & Carraro, G. 2004, ApJ, 605, L125
Bedin, L.R., Piotto, G., Zoccali, M., Stetson, P.B., Saviane, I., Cassisi, S., & Bono, G. 2000, A&A, 363, 159
Behr, B.B. 2003, ApJS, 149, 67
Bellini, A., Anderson, J., Salaris, M., Cassisi, S., Bedin, L.R., Piotto, G., & Bergeron, P. 2013a, ApJ, 769, L32
Bellini, A., et al. 2013b, ApJ, 765, 32
Brown, T.M., Lanz, T., Sweigart, A.V., Cracraft, M., Hubeny, I., & Landsman, W.B. 2012, ApJ, 748, 85
Brown, T.M., Sweigart, A.V., Lanz, T., Landsman, W.B., & Hubeny, I. 2001, ApJ, 562, 368
Brown, T.M., Sweigart, A.V., Lanz, T., Smith, E., Landsman, W.B., & Hubeny, I. 2010, ApJ, 718, 1332
Busso, G., et al. 2007, A&A, 105, 119
Caloi, V., & D'Antona, F.D. 2007, A&A, 463, 949
Carretta, E. 2015, ApJ, 810, 148
Carretta, E., Bragaglia, A., Gratton, R., D'Orzai, V., & Lucatello, S. 2009, A&A, 508, 695
Cassisi, S., & Salaris, M. 2013, in Old Stellar Populations: How to Study the Fossil Record of Galaxy Formation (Berlin: Wiley)
Cassisi, S., Schlattl, H., Salaris, M., & Weiss, A. 2003, ApJ, 582, L43
Castelli, F., & Kurucz, R.L. 2003, in IAU Symposium 210, Modeling of Stellar Atmospheres, eds. N. Piskunov, W.W. Weiss, & D.F. Gray, poster A20, astro-ph/0405087
Catelan, M. 2009, Ap&SS, 320, 261
Catelan, M., Borissova, J., Sweigart, A.V., & Spassova, N. 1998, ApJ, 494, 265
Caughlan, G.R., & Fowler, W.A. 1988, At. Data Nucl. Data Tables, 40, 283
Corwin, T.M., Sumerel, A.N., Pritzl, B.J., Smith, H.A., Catelan, M., Sweigart, A.V., & Stetson, P.B. 2006, AJ, 132, 1014
D'Antona, F., Bellazzini, M., Caloi, V., Pecci, F.F., Galleti, S., & Rood, R.T. 2005, ApJ, 631, 868
D'Antona, F., & Caloi, V. 2004, ApJ, 611, 871
D'Antona, F., & Caloi, V. 2008, MNRAS, 390, 693
D'Cruz, N.L., Dorman, B., Rood, R.T., & O'Connell, R.W. 1996, ApJ, 466, 359
D'Cruz, N.L., O'Connell, R.W., Rood, R.T., Whitney, J.H., Dorman, B., Landsman, W.B., Hill, R.S., Stecher, T.P., & Bohlin, R.C. 2000, ApJ, 530, 352
Dalessandro, E., Lanzoni, B., Ferraro, F.R., Rood, R.T., Milone, A., Piotto, G., & Valenti, E. 2008, ApJ, 677, 1069
Dalessandro, E., Salaris, M., Ferraro, F.R., Cassisi, S., Lanzoni, B., Rood, R.T., Fusi Pecci, F., & Sabbi, E. 2011, MNRAS, 410, 694
Dalessandro, E., Salaris, M., Ferraro, F.R., Mucciarelli, A., & Cassisi, S. 2013, MNRAS, 430, 459
Dieball, A., Knigge, C., Maccarone, T.J., Long, K.S., Hannikainen, D.C., Zurek, D., & Shara, M. 2009, MNRAS, 394, L56
Dieball, A., Long, K.S., Knigge, C., Thomson, G.S., & Zurek, D.R. 2010, ApJ, 710, 332
Ferraro, F.R., Paltrinieri, B., Fusi Pecci, F., Rood, R.T., & Dorman, B. 1998, ApJ, 500, 311
Ferraro, F.R., Sollima, A., Pancino, E., Bellazzini, M., Straniero, O., Origlia, L., & Cool, A.M. 2004, ApJ, 603, L81
Fitzpatrick, E.L. 1999, PASP, 111, 63
Geier, S., Heber, U., Edelmann, H., Morales-Rueda, L., & Napiwotzki, R. 2010, Ap&SS, 329, 127
Girardi, L., Castelli, F., Bertelli, G., & Nasi, E. 2007, A&A, 468, 657
Gratton, R.G., et al. 2012, A&A, 539, A19
Gratton, R.G., Lucatello, S., Carretta, E., Bragaglia, A., D'Orazi, V., & Momany, Y. Al 2011, A&A, 534, A123
Grundahl, F., Catelan, M., Landsman, W.B., Stetson, P.B., & Andersen, M.I. 1999, ApJ, 524, 242
Grundahl, F., VandenBerg, D.A., & Andersen, M.I. 1998, ApJ, 500, L179
Harris, W.E. 1996, AJ, 112, 1487
Kurucz, R.L. 1993, CD-ROM 13, 18, http://kurucz.harvard.edu
Layden, A.C., Ritter, L.A., Welch, D.L., & Webb, T.M.A. 1999, AJ, 117, 1313
Layden, A.C., & Sarajedini, A. 2000, AJ, 119, 1760
Marino, A.F., et al. 2014, MNRAS, 437, 1609
Michaud, G., Richer, J., & Richard, O. 2007, ApJ, 670, 1178
Michaud, G., Richer, J., & Richard, O. 2008, ApJ, 675, 1223
Michaud, G., Richer, J., & Richard, O. 2011, A&A, 529, A60

Milone, A.P., et al. 2012, ApJ, 744, 58
Milone, A.P., et al. 2013, ApJ, 767, 120
Milone, A.P., et al. 2014, ApJ, 785, 21
Milone, A.P., et al. 2015a, MNRAS, 447, 927
Milone, A.P., et al. 2015b, ApJ, 808, 51
Moehler, S. 2001, PASP, 113, 1162
Moehler, S., Dreizler, S., Lanz, T., Bono, G., Sweigart, A.V., Calamida, A., & Nonino, M. 2011, A&A, 526, A136
Moehler, S., Sweigart, A.V., Landsman, W.B., & Heber, U. 2000, A&A, 360, 120
Moehler, S., Sweigart, A.V., Landsman, W.B., Heber, W.B., & Catelan, M. 1999, A&A, 346, L1
Momany, Y., Bedin, L.R., Cassisi, S., Piotto, G., Ortolani, S., Recio-Blanco, A., De Angeli, F., & Castelli, F. 2004, A&A, 420, 605
Momany, Y., Piotto, G., Recio-Blanco, A., Bedin, L.R., Cassisi, S., & Bono, G. 2002, ApJ, 576, L65
Moni Bidin, C., Moehler, S., Piotto, G., Momany, Y., & Recio-Blanco, A. 2007, A&A, 474, 505
Pace, G., Recio-Blanco, A., Piotto, G., & Momany, Y. 2006, A&A, 452, 493
Pietrinferni, A., Cassisi, S., Salaris, M., Percival, S., & Ferguson, J. 2009, ApJ, 697, 275
Piotto, G., et al. 2002, A&A, 391, 945
Piotto, G., et al. 2015, AJ, 149, 91
Piotto, G., Bedin, L.R., Anderson, J., King, I.R., Cassisi, S., Milone, A.P., Villanova, S., Pietrinferni, A., & Renzini, A. 2007, ApJ, 661, L53
Piotto, G., Milone, A.P., Anderson, J., Bedin, L.R., Bellini, A., Cassisi, S., Marino, A.F., Aparacio, A., & Nascimbeni, V. 2012, ApJ, 760, 39
Pritzl, B.J., Smith, H.A., Catelan, M., & Sweigart, A.V. 2000, ApJ, 530, L41
Pritzl, B.J., Smith, H.A., Catelan, M., & Sweigart, A.V. 2001, AJ, 122, 2600
Pritzl, B.J., Smith, H.A., Catelan, M., & Sweigart, A.V. 2002, AJ, 124, 949
Pritzl, B.J., Smith, H.A., Stetson, P.B., Catelan, M., Sweigart, A.V., Layden, A.C., & Rich, R.M. 2003, AJ, 126, 1381
Quievy, D., Charbonneau, P., Michaud, G., & Richer, J. 2009, A&A, 1163, 1171
Recio-Blanco, A., Piotto, G., Aparicio, A., & Renzini, A. 2002, ApJ, 572, L71
Recio-Blanco, A., Piotto, G., Aparicio, A., & Renzini, A. 2004, A&A, 417, 597
Renzini, A., et al. 2015, MNRAS, in press, arxiv/1501.01468
Rich, R.M., et al. 1997, ApJ, 484, L25
Robertson, J.W., & Faulkner, D.J. 1972, ApJ, 171, 309
Rogers, F.J., & Iglesias, A.C. 1992, ApJS, 79, 507
Sandage, A., & Wallerstein, G. 1960, ApJ, 131, 598
Sandage, A., & Wildey, R. 1967, ApJ, 150, 469
Sbordone, L., Bonifacio, P., Castelli, F., & Kurucz, R.L. 2004, MSAIS, 5, 93
Sbordone, L., Salaris, M., Weiss, A., & Cassisi, S. 2011, A&A, 534, A9
Schwarzschild, M., & Härm, R. 1965, ApJ, 142, 855
Siegel, M.H., et al. 2007, ApJ, 667, L57
Sosin, C., et al. 1997, ApJ, 480, L35
Sweigart, A.V. 1987, ApJS, 65, 95
Sweigart, A.V. 1997, ApJ, 474, L23
Sweigart, A.V. 1997, in The Third Conference on Faint Blue Stars, ed. A.G.D. Phillip, J. Liebert, & R.A. Saffer (Schenectady: L. Davis Press), 3
Sweigart, A.V. 2002, in Highlights of Astronomy 12, ed. H. Rickman (San Francisco: ASP), 292
Sweigart, A.V., & Demarque, P. 1972, A&A, 20, 445
Sweigart, A.V., & Gross, P.G. 1974, ApJ, 190, 101
Sweigart, A.V., & Gross, P.G. 1976, ApJS, 32, 367
Sweigart, A.V., & Gross, P.G. 1978, ApJS, 36, 405
Valcarce, A.A.R., Catelan, M., & Sweigart, A.V. 2012, A&A, 547, A5
van den Bergh, S. 1967, AJ, 72, 70
Walker, A.R. 1999, AJ, 118, 432
Weaver, T.A., & Woosley, S.E. 1993, Phys. Rep., 227, 65
Zinn, R., & West, M.J. 1984, ApJS, 55, 45